Magmatic architecture below the Okataina Volcanic Centre, Taupō Volcanic Zone, Aotearoa New Zealand, inferred from basalt geochemistry

Ery C. Hughes: Te Pū Ao | GNS Science (e.hughes@gns.cri.nz)

Sally Law: School of GeoSciences, University of Edinburgh (Sally.Law@ed.ac.uk)

Geoff Kilgour: Te Pū Ao | GNS Science (g.kilgour@gns.cri.z)

Jon D. Blundy: University of Oxford (jonathan.blundy@earth.ox.ac.uk)

Heidy M. Mader: University of Bristol (h.m.mader@bristol.ac.uk)

This paper is a non-peer review pre-print submitted to EarthArXiv, which has been submitted to the Journal of Volcanology and Geothermal Research special issue on the Okataina Volcanic Centre for peer review.

Twitter handles: @eryhughes, @sallylaw, @NZvolcanologist

Abstract

The Okataina Volcanic Centre (OVC) is the most recently active rhyolitic volcanic centre in the Taupō Volcanic Zone, Aotearoa New Zealand. Although best known for its high rates of explosive rhyolitic volcanism, there are numerous examples of basaltic to basaltic-andesite contributions to OVC eruptions, ranging from minor involvement of basalt in rhyolitic eruptions to the exclusively basaltic 1886 C.E. Plinian eruption of Tarawera. To explore the basaltic component supplying this dominantly rhyolitic area, we analyse the textures and compositions (minerals and melt inclusions) of four basaltic eruptions within the OVC that have similar whole rock chemistry, namely: Terrace Rd, Rotomakariri, Rotokawau, and Tarawera. Data from these basaltic deposits provide constraints on the conditions of magma evolution and ascent in the crust prior to eruption, revealing that at least five different magma types (two basalts, two dacites, one rhyolite) are sampled during basaltic eruptions. The most abundant basaltic magma type is generated by cooling-induced crystallisation of a common, oxidised, basaltic melt at various depths throughout the crust. The volatile content of this melt was increased by protracted fluid-undersaturated crystallisation. All eruptions display abundant evidence for syn-eruptive mixing of the different magma types. Rotomakariri, consisting of a mafic crystal cargo mixed into a dacitic magma is the most extreme example of this process. Despite similar bulk compositions, comparable to other basaltic deposits in the region, these four OVC eruptions are texturally distinct as a consequence of their wide variation in eruption style.

Keywords: geochemistry, Tarawera, Terrace Rd, Rotomakariri, Rotokawau, melt inclusion

1 Introduction

Volcanic arcs are characterised by complicated sub-surface architectures that convert basaltic mantle-derived melt into a wide variety of more evolved arc magma compositions (e.g., reviews by Ducea et al., 2015; Grove et al., 2012). The compositional variability can be derived from variations in the composition of the mantle melt input, extents of crustal assimilation, type of petrological processes occurring (e.g., crystallisation, degassing, mixing), and the conditions of magma stagnation (i.e., pressure and temperature). Static models drive compositional variation by changes in temperature (e.g., Annen et al., 2006), whereas dynamic models drive compositional variation by reactive melt percolation (e.g., Jackson et al., 2018); both mechanisms have been used to explain the compositional variability at arcs. Reconciling these models requires observations and analysis of volcanic rocks or exhumed crustal sections, which provide snapshots and time-integrated histories, respectively, of magmatic systems.

The crustal and erupted material at arcs is dominated by evolved magma composition (i.e., andesites to rhyolites) despite the large inputs of basaltic melt required for their formation. Most basalts never reach the surface due to relatively high magma density. Furthermore, these intrusions cool in the crust and either solidify to gabbroic plutons or generate more evolved magmas that separate and erupt or cool to form plutons. Periodic magma mixing (e.g., basalt with rhyolite) may be important in generating intermediate magmas and triggering eruptions (e.g., Laumonier et al., 2014; Sparks et al., 1977). Any basaltic magmas that do reach the surface will have traversed this complicated crustal region, yet unravelling this cryptic history is not trivial and inevitably requires high resolution, *in situ* mineral analysis. Here, we utilise microanalytical geochemical methods to collect data on crystals and their melt inclusions to explore the paths taken by basaltic magmas in a dominantly rhyolitic caldera. We aim to constrain how and where basaltic magmas are stored within the crust, and what petrological

processes affect them. This is important for assessing the current state of magma reservoirs in the crust through geophysical surveys and predicting potential precursory signals before a future eruption at caldera systems.

The Okataina Volcanic Centre (OVC) is one of two (Taupō Volcanic Centre is the other) currently active caldera systems in the Taupō Volcanic Zone, Aotearoa New Zealand. From several studies of the rhyolites, the sub-surface architecture below the OVC is known to comprise discrete rhyolitic melt-mush pockets that erupt compositionally distinct magmas within single eruptions (e.g., Cole et al., 2014; Sas et al., 2021; Shane et al., 2008a, 2007; Smith et al., 2004; Storm et al., 2011). Basaltic magmas are key to generating the more evolved magma compositions in the OVC, but little is known about their evolution. Heat and volatiles are assumed to be transferred between basalts and rhyolites to trigger rhyolitic eruptions (e.g., Leonard et al. 2002; Shane et al. 2007, 2008; Smith et al. 2010), but the initial volatile contents of the basaltic magmas are unconstrained. The abundant evidence for basaltic-rhyolitic magma interaction also enables the investigation of how magma mixing is related to basaltic eruption style (e.g., Leonard et al., 2002; Shane et al., 2005). In this study, we combine textural observations with mineral and melt inclusion chemistries to constrain the magmatic compositions (including volatiles), conditions, and processes occurring during crustal storage and ascent of OVC basaltic magmas. These data are then used to derive a model for the magmatic architecture of the OVC.

2 Regional setting

The Taupō Volcanic Zone (TVZ) is the most frequently active and productive silicic system on Earth. Oblique subduction of the Pacific plate under continental Zealandia leads to the clockwise rotation of the eastern portion of the North Island, resulting in extension in the TVZ, crustal thinning, and basalt underplating (Houghton et al., 1995; Mortimer et al., 2017; Wilson et al., 1995). High rates of basaltic underplating drive the generation of voluminous silicic magma and, together with the relatively thin and faulted crust, enhance magma production and the high frequency of eruptions (e.g., Cole et al., 2014; Price et al., 2005). Extensive crustal contamination occurs, which influences the isotopic composition of both erupted basalts and rhyolites (e.g., Gamble et al., 1993; Graham et al., 1995; Sas et al., 2021).

Basalt scoria cones and tuffs are volumetrically minor surface features, being one and two-to-three orders of magnitude less voluminous than andesites/dacites and rhyolites, respectively (Wilson et al., 1995). Basalts of the TVZ are classified as high-alumina and are generated by a combination of rift-induced decompression melting and fluid-induced flux melting (Hiess et al., 2007; Law et al., 2021). Active calderas have high inputs of basalt from the mantle wedge, which is caused by fluid-fluxed melting of fertile mantle: i.e., mantle that has not undergone much previous melting (Barker et al., 2020; Zellmer et al., 2020). The mantle source is lherzolitic as the sub-continental lithospheric mantle found further south in the TVZ has been removed by rifting and crustal thinning, causing the shift to rhyolitic rather than andesitic volcanism (Law et al., 2021). Regions without active calderas have lower inputs of basalt due to either a subdued influence from fluid-fluxing or a more depleted mantle source (Barker et al., 2020; Zellmer et al., 2020). In the latter mechanism, the depleted source is caused by prior melt extraction associated with caldera formation in the region, but these calderas are no longer active (Zellmer et al., 2020). Basaltic eruptions throughout the TVZ are often associated with faults and commonly erupt in association with rhyolitic magmas (Cole, 1970a; Hiess et al., 2007; Nairn and Cole, 1981). Basaltic volcanism exhibits a wide range of eruption style, both within and between individual eruptions and volcanic centres, and shallow conduit processes

(including interaction with external, non-magmatic water) are thought to play a major role in determining eruption style (e.g., Carey et al., 2007; Houghton and Hackett, 1984).

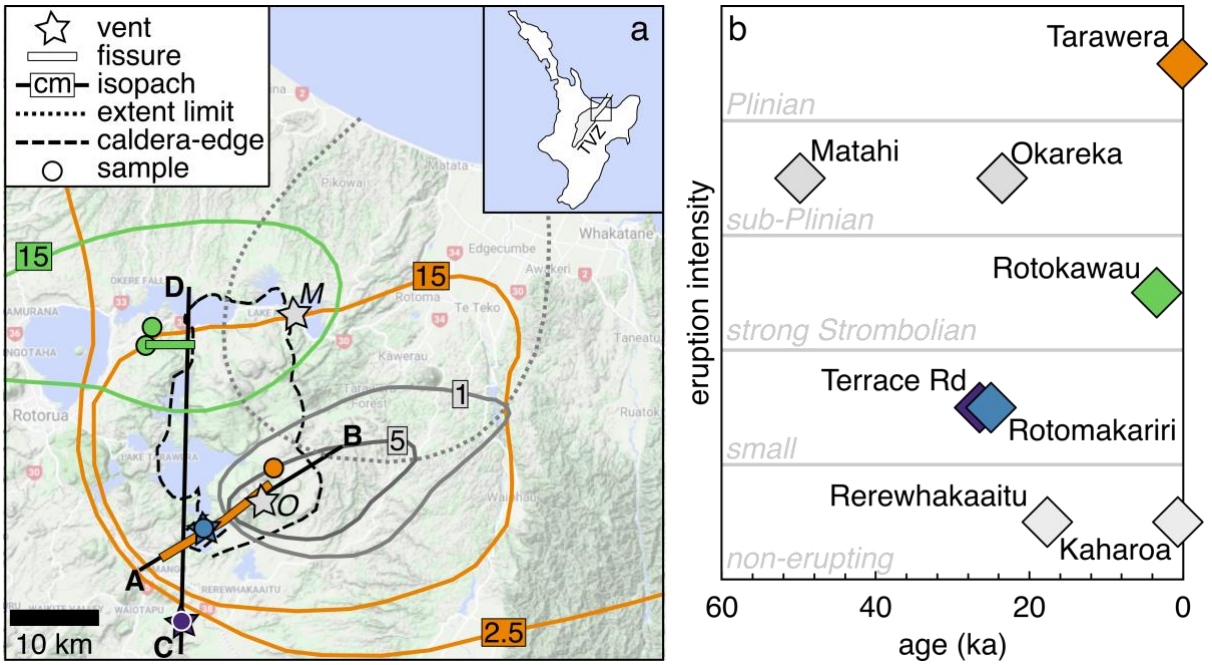

Figure 1 **(a)** Map of the Okataina Volcanic Centre (OVC) showing the location of eruptive vents and fissures (Beanland, 1989; Burt et al., 1998; Darragh et al., 2006; Nairn, 2002, 1992); deposit thickness isopleths or extent limit (Beanland, 1989; Darragh et al., 2006; Nairn, 1992; Pullar and Nairn, 1972); sample locations for this study for the basaltic eruptions (colours shown in (b) – eruptions analysed in this study are in colour and other OVC basalts are shown in grey); and the locations of schematic cross-sections AB and CD shown in Figure 6 (heavy black solid lines), with an inset showing the location of the main map and the Taupō Volcanic Zone (TVZ, shaded area) in the North Island of Aotearoa New Zealand. *M* = Matahi, where the dotted-grey line is the extent limit; and *O* = Okareka, where the solid-grey lines are the 1 and 5 cm isopachs. **(b)** Qualitative eruption intensity against age (Hopkins et al., 2021; Nairn, 2002) for OVC basaltic magmas – Rerewhakaaitu and Kaharoa do not appear in (a) because they only occur as basaltic enclaves and blebs within a rhyolitic eruption.

The geology of the currently active OVC is overwhelmingly rhyolitic, but a diverse range of styles and intensities of basaltic explosive activity is also present (Cole et al., 2014; Nairn, 2002) (Figure 1a). Since ~55 ka there have been at least six basaltic eruptions (and additionally two examples of mafic enclaves and blebs in entirely rhyolitic eruptions) ranging from phreatomagmatic to magmatic and Strombolian to Plinian in intensity (Table 1 and Figure 1) (Cole et al., 2014; Nairn, 2002). Basaltic Plinian eruptions are rare in the geological record and Tarawera is the most recent (Cole, 1970a; Nairn, 1979; Rowe et al., 2021; Thomas, 1888; Walker et al., 1984). Only two other volcanoes globally have documented examples of such eruptions: Masaya (Nicaragua; Williams, 1983) and Etna (Italy; Coltelli et al., 1998).

Basaltic eruptions in the OVC are fed by dikes with their vents often aligned along the main tectonic fabric (i.e., with a strike trending NE-SW), predominantly located on the Tarawera Linear Vent Zone, but are also found just outside the caldera boundaries (Nairn, 2002) (Figure 1a). Most individual eruptions issued from a single vent, but the Tarawera and Rotokawau eruptions occurred along fissures, displaying a range of style and intensity both spatially and temporally within each eruption (Nairn, 2002). For instance, the Tarawera eruption generated a ~17 km NE-SW fissure, with Strombolian to Plinian magmatic eruptions in the NE and

phreatomagmatic eruptions in the SW where it intersected an active hydrothermal system, (Nairn, 1979; Nairn and Cole, 1981; Walker et al., 1984). The Tarawera fissure is broadly aligned with the TVZ extension direction, which contrasts markedly to the Rotokawau eruption where the fissure strikes E-W (Beanland, 1989). Additionally, many of the OVC rhyolitic eruptions are likely triggered by the injection of basaltic magmas (e.g., Leonard et al., 2002; Shane et al., 2008, 2007). Some rhyolitic eruptions were preceded by basaltic eruptions, with either no (e.g., Matahi prior to Rotoiti) or direct (e.g., mixed basaltic-rhyolitic clasts in Okareka) evidence for magma mixing prior to eruption, whereas others (e.g., Rerewhakaaitu and Kaharoa) host basaltic blebs and enclaves (e.g., Burt et al., 1998; Cole, 1973a; Cole et al., 2014; Leonard et al., 2002; Nairn, 1992; Pullar and Nairn, 1972; Schmitz and Smith, 2004; Shane et al., 2007, 2008a). The OVC is passively degassing CO_2 and heat today and inferred basaltic dike events also occur (e.g., Benson et al., 2021; Hughes et al., 2019b; Mazot et al., 2014).

Table 1 Okataina Volcanic Centre (OVC) basaltic eruptions and magmas since the last caldera-forming eruption.

Eruption	Age (ka)	Description	DRE volume (km^3) [Column height (km)]
Tarawera*	1886 C.E.	Phreatomagmatic to magmatic, Strombolian to Plinian fissure[1–3]	0.25–0.48[4] [~28][3]
Kaharoa	0.6[5]	Enclaves in rhyolitic eruption[6–8]	>0.01[8]
Rotokawau*	3.44 ± 0.07[11]	Phreatomagmatic (Surtseyan) and Strombolian fissure[9–11]	0.55[9] [4.5–7][9]
Rerewhakaaitu	17.6[5]	Blebs in rhyolitic eruption[12]	n.d.
Okareka	23.5[5]	Single vent, sub-Plinian phase prior to rhyolitic eruption[13–14]	0.01[13,15]
Rotomakariri*	22–28[11]	Single vent tuff cone[11]	n.d.
Terrace Rd*	25–28, 28 ± 2[11]	Single vent (?), small phreatomagmatic[11]	n.d.
Matahi†	~45–55[5]	Single vent, sub-Plinian[16]	<1[17]

Notes: *Eruptions analysed in this study. †The Matahi eruption occurred just prior to the Rotoiti Ignimbrite that was the most recent OVC caldera-forming eruption. The volumes (DRE = dense rock equivalent) for Terrace Rd and Rotomakariri are not determined (n.d.), but are likely very small due to their limited occurrence (Nairn, 2002). References: [1]Keam (1988), [2]Nairn and Cole (1981), [3]Walker et al. (1984), [4]Rowe et al. (2021), [5]Hopkins et al. (2021), [6]Leonard et al. (2002), [7]Nairn et al. (2001), [8]Nairn et al. (2004), [9]Beanland (1989), [10]Beanland and Houghton (1978), [11]Nairn (2002), [12]Shane et al., (2007), [13]Darragh et al. (2006), [14]Nairn (1992), [15]Shane et al. (2008a), [16]Pullar and Nairn (1972), and [17]Froggatt and Lowe (1990).

All OVC basalts (including blebs in rhyolitic eruptions) contain olivine, clinopyroxene, and plagioclase crystals (sometimes in aggregates) within a glassy (e.g., Matahi) to highly microcrystalline groundmass (e.g., Cole, 1970b; Law et al., 2021; Nairn, 2002, 1992; Rowe et al., 2021; Sable et al., 2009; Schmitz and Smith, 2004; Shane et al., 2008a). Additionally, all basalts contain xenocrystic quartz and rhyolitic material entrained during ascent (Beanland, 1989; Cole, 1973a; Nairn, 2002; Schmitz and Smith, 2004). Hornblende has only been observed in basaltic enclaves in the Kaharoa eruption in the OVC since ~55 ka (Leonard et al., 2002). Clast vesicularity ranges from dense to highly vesicular, even within an eruption (Beanland, 1989; Nairn, 2002; Shane et al., 2008a). Dense clasts are often used as evidence for interaction with external water leading to increased eruption intensity (e.g., Beanland and Houghton, 1978; Carey et al., 2007).

3 Methods

We sampled and analysed material from the Terrace Rd, Rotomakariri, Rotokawau, and Tarawera eruptions as they cover the full range of eruption styles and sizes (phreatomagmatic to magmatic and Strombolian to Plinian) observed in the OVC (Figure 1b). All eruptions occurred in an active caldera region, but Rotomakariri and Tarawera occurred inside the caldera boundary (along one of the main linear vent zones), whereas Terrace Rd and Rotokawau occurred just outside the caldera boundary (Figure 1a). Additionally, there are no published melt inclusion data for Terrace Rd, Rotomakariri, and Rotokawau, and only limited published data for Tarawera (Barker et al., 2020; Rowe et al., 2021), whereas melt inclusions have been previously analysed from Okareka and Kaharoa (Barker et al. 2020).

Samples were collected during three fieldwork seasons between 2015 and 2017 (Figure 1a). Localities for deposits for the Terrace Rd, Rotomakariri, and Rotokawau eruptions were taken from Nairn (2002); exact sample locations and descriptions are given in Supplementary Material (including for Tarawera samples). For Tarawera, samples were collected off the volcano to avoid material that had cooled slowly, which can enhance post-entrapment crystallisation of melt inclusions (e.g., Lloyd et al., 2013). Samples were dried in a low-temperature oven then sieved into 1 φ size fractions. The clast densities for -3 to -6 φ from Terrace Rd, -4 to -5 φ from Rotomakariri, -3 to -4 φ from Rotokawau, and -4 to -5 φ from Tarawera were measured using the method of Houghton and Wilson (1989). Vesicularity was calculated assuming the rock density was equal to an anhydrous melt density (assumed to approximate the glass density) with the composition of the average whole rock data from the literature (given in Supplementary Material) at room temperature and pressure using DensityX (Iacovino and Till, 2018). Two mean density samples were chosen to make thin sections from (random samples were selected for Rotokawau from a different location due to the small clast size sampled during our fieldwork).

To constrain pre-eruptive magmatic compositions, conditions, and processes for these eruptions, we analysed mineral and melt inclusion chemistry and textures. Scoria -2 to -3 φ in size were selected to ensure rapid clast cooling, thereby increasing the potential for glassy melt inclusions that had retained their initial volatile content (Lloyd et al., 2013). Olivine, pyroxene, and plagioclase crystals were hand-picked from gently crushed clasts and either bulk mounted in epoxy or individually mounted and polished to expose a melt inclusion at the surface. Both types of mounts were polished to ~1 μm using diamond-paste. Only naturally glassy melt inclusions were analysed; no rehomogenisation experiments were carried out.

Olivine, pyroxene, and plagioclase mineral separates were analysed using electron probe micro-analysis (EPMA) wavelength dispersive spectrometry (WDS). Melt inclusions from all eruptions were analysed using EPMA-WDS for major, minor, and volatile (S, Cl, and F) elements and for H_2O using calibrated volatiles-by-difference (Hughes et al., 2019a). A subset of melt inclusions from Tarawera was analysed for H_2O and CO_2 using secondary ion mass spectrometry (SIMS) prior to EPMA. To put mineral separate data into context, textural observations on thin sections were made using optical microscopy and scanning electron microscopy (SEM). Some mineral phases (and the groundmass glass for Rotomakariri) in the thin sections were analysed using semi-quantitative (sq) SEM energy dispersive spectroscopy (EDS) (sq-SEM-EDS) and EPMA-WDS to correlate the textures with mineral separates data.

Several thermometers (melt, olivine-melt, clinopyroxene-melt, and clinopyroxene-orthopyroxene; Putirka, 2008), oxybarometers (melt Fe^{3+}/Fe_T; Kress and Carmichael, 1991), and barometers (clinopyroxene-melt; Neave and Putirka, 2017, and H_2O-CO_2 melt concentrations; Mangan et al., 2021) were applied to mineral, melt inclusion, and whole rock data from this study and the literature. Full analytical and calculation details are in

Supplementary Material. Data collection and reporting for melt inclusions broadly follows the guidelines of Rose-Koga et al. (2021).

4 Textural and chemical characteristics

Texturally and chemically, Tarawera, Rotokawau, and Terrace Rd scoria are more similar to each other than to scoria from Rotomakariri. All data collected are provided in Supplementary Material.

4.1 Vesicles, groundmass, and macrocrysts

Tarawera, Rotokawau, and Terrace Rd are characterised by vesicles (~41–48 vol%) with complex shapes in a highly crypto- to microcrystalline groundmass containing olivine, clinopyroxene, plagioclase, and Fe-Ti oxides (Figure 2a, c, and d). Although the size and proportions of the groundmass phases vary slightly between these eruptions, the main difference is that Tarawera is much more microcrystalline than Rotokawau and Terrace Rd (i.e., >90 groundmass area% of scoria at Tarawera compared to 60 area% at Terrace Rd). In detail, groundmass olivine is <10–200 μm at Rotokawau (6 area%) and Terrace Rd (22 area% and euhedral) but <30 μm and hopper-shaped at Tarawera (14 area%). Clinopyroxene is 6 area% at Terrace Rd but 27–28 % at Tarawera (<20 μm) and Rotokawau (10–100 μm). Plagioclase is <10–200 μm (67 area% at Rotokawau) and needle- to swallowtail-shaped at Tarawera (55 area%), but acicular to tabular at Terrace Rd (72 area%). Oxides are always a minor, small groundmass phase (<2 area%, <5 μm).

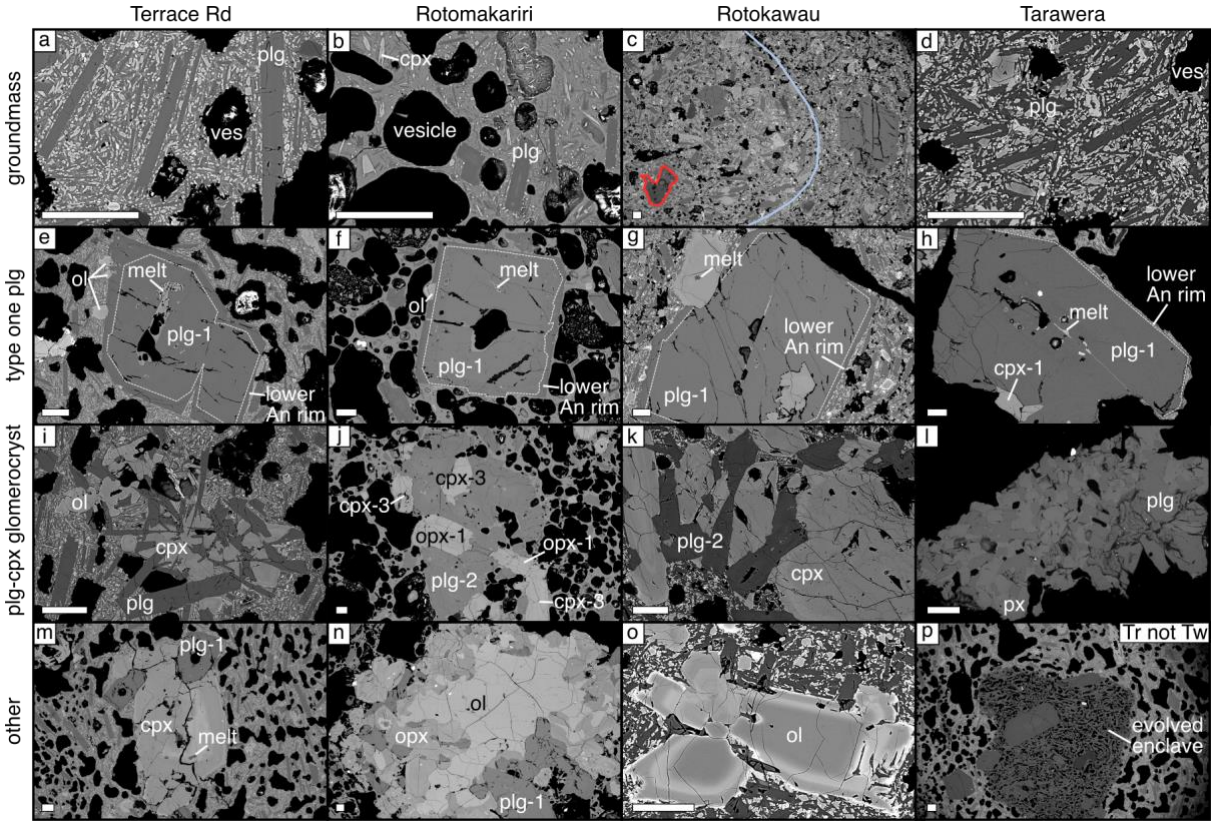

Figure 2 Annotated back-scattered electron (BSE) scanning electron microscope (SEM) images of scoria textures, where the white bar in the bottom left of each image is 100 μm in length. Each column is an eruption: Terrace Rd (a, e, i, m, and additionally p in the far-right column), Rotomakariri (b, f, j, and n), Rotokawau (c, g, k, and o), and Tarawera (d, h, and l: note the bottom image p is for Terrace Rd). Different features are shown in each row: **(a–d)** groundmass textures, where in **(b)** plagioclase is An_{76}, and **(c)** shows alignment of plagioclase from basalt-basalt magma mixing (blue line) and a region of evolved material is outlined in red; **(e–h)** type one plagioclase with high An cores ($An_{93–96}$) and lower An rims ($An_{76–87}$), which have other phases attached to make glomerocrysts; **(i–m)** glomerocrysts of plagioclase and pyroxene: **(i)** type Tr-B with plagioclase, clinopyroxene, and altered olivine on the edge; **(j)** type Rm-B glomerocryst with high An plagioclase (core is An_{83}, rim is An_{79} using sq-EDS), clinopyroxene (Mg# 75–78), and orthopyroxene (Mg# = 71 core, 75 rim); **(k)** clinopyroxene (Mg# 85) and plagioclase (An_{88}); **(l)** intergrown plagioclase and pyroxene; **(m)** type Tr-C with plagioclase and olivine grains (Fo_{76}) attached to a clinopyroxene (Mg# = 65 core, 80 middle, 73 rim); and **(n–p)** other textures: **(n)** type Rm-A glomerocryst: centre is a partially resorbed olivine (Fo_{83}), with overgrowths of orthopyroxene (Mg# 76), plagioclase (An_{92} core, An_{85} rim), and some clinopyroxene on the outer portion; **(o)** olivine macrocryst (dark portions are Fo_{80}, bright band is Fo_{75}); and **(p)** evolved enclave containing type three plagioclase and quartz, with some evidence of reacting with the basaltic melt around the edges (note this is from Terrace Rd, not Tarawera). *Abbreviations:* ves = vesicle, ol = olivine, plg = plagioclase, cpx = clinopyroxene, opx = orthopyroxene, px = pyroxene.

Rotokawau and Tarawera scoria are homogeneously brown-to-black, whereas Terrace Rd is highly variable in colour (black to light-brown), including small domains (<3 mm across) of black and grey material. At Terrace Rd, the groundmass is very similar in both the brown and black areas, although plagioclase microlites are slightly shorter in the black material. When in contact, microlites in the brown groundmass are flow-aligned around the edge, whilst the margins of the black groundmass are crenulated and wavy. Rotokawau also shows multiple

groundmass textures, including flow alignment (Figure 2c). One Tarawera thin section contains a light grey band (1.5 × 0.5 cm across) that is glassy, non-vesicular, banded, and has sharp, clear edges in contact with the basaltic groundmass.

Rotomakariri scoria are homogeneously brown-to-black and have rounded vesicles (~48 vol%) in a groundmass (~20 area% of the scoria) of glass (54 area% of groundmass) containing sparse microlites of plagioclase (38 area%, <5–100 μm) and clinopyroxene (8 area%, <20 μm) (Figure 2b).

Terrace Rd, Rotokawau, and Rotomakariri contain abundant macrocrysts, mostly as glomerocrysts, whereas Tarawera is almost macrocryst- and glomerocryst-free (see also Law et al., 2021). All eruptions have a similar mineralogy of olivine (~10–15 area%), plagioclase (~50 area%), and clinopyroxene (~20–25 area%), with Rotomakariri additionally containing abundant orthopyroxene (~20 area%). Alkali feldspars and quartz were found in all eruptions, including an alkali feldspar inclusion in orthopyroxene at Tarawera.

Olivine composition is variable between eruptions, with a narrow range in forsterite content at Terrace Rd (78.3 ± 0.4) and Tarawera (81.9 ± 0.6) and a wide range (72–82) at Rotomakariri and Rotokawau (Figure 3a–e). Based on minor element chemistry (NiO and CaO) and Fo, Law et al. (2021) defined olivines from Terrace Rd, Tarawera, and Rotokawa as group 1 and those from Rotomakariri as group 2, which is supported by this data. Groundmass olivine from Tarawera analysed by Rowe et al. (2021) has a lower forsterite content than the macrocrystals (Figure 3a). In Rotokawau, olivine (50–150 μm in size) is weakly zoned and the outer regions often display dendritic growth (Figure 2o). In Rotomakariri, single olivine grains are rare, and large grains (150 μm in size) have an overgrowth of many small orthopyroxene crystals, consistent with type 2 olivine in Law et al. (2021).

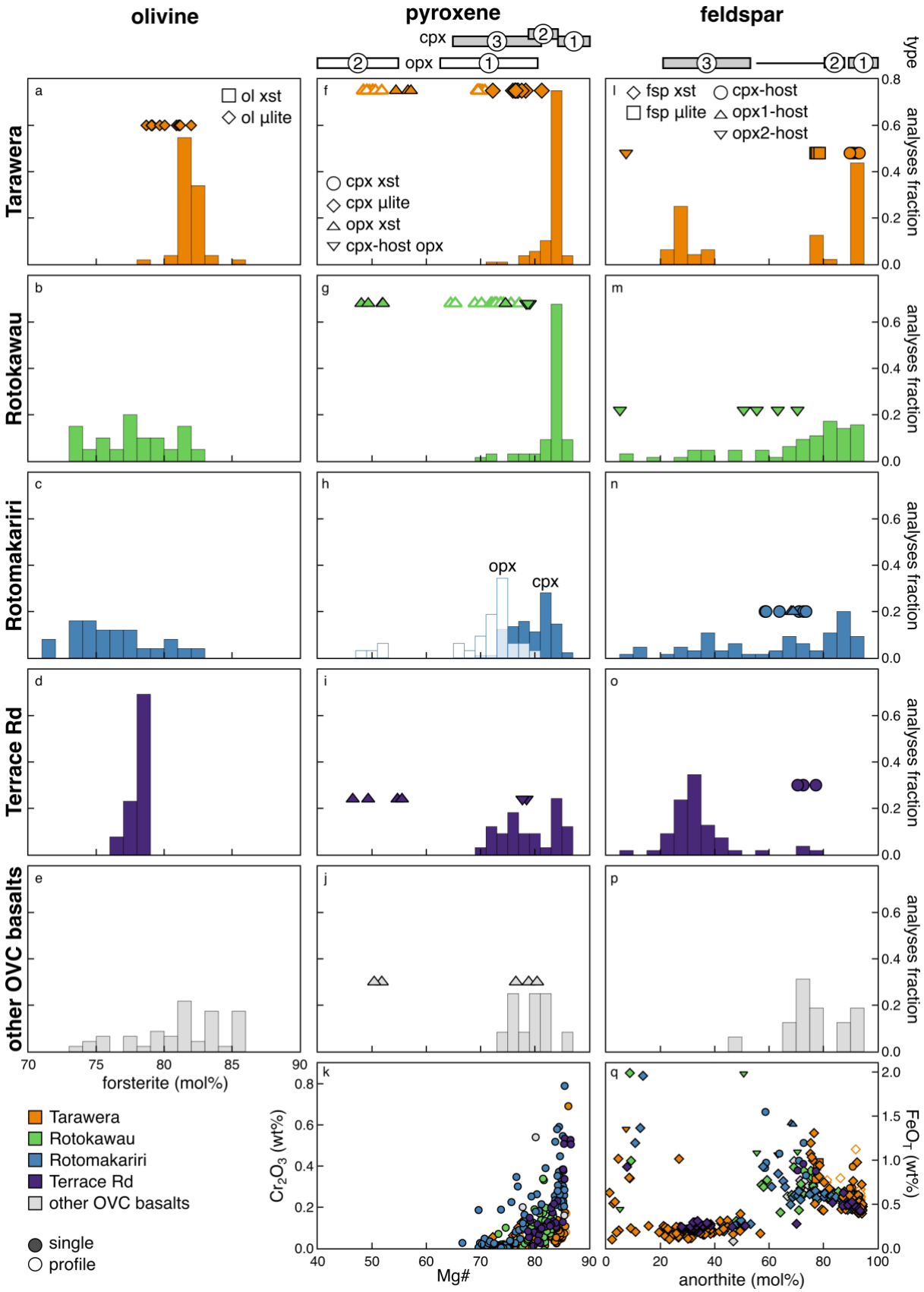

Figure 3 Summary of the mineral chemistry for OVC basalts. Histograms **(a–e, f–j, i–p)** show the fraction of analyses in each compositional bin (data from profiles across grains are not included in the histogram; e.g., only core analyses from Rowe et al. (2021) and Law et al. (2021) are included), with additional individual analyses shown as symbols. Each column

represents a different mineral phase, which are labelled along the top: **(a–e)** olivine – fosterite content, **(b–j)** pyroxene – Mg# (histograms are for cpx, except unfilled bars in **(h)** that are for opx), and **(l–p)** feldspar – anorthite content. Each row represents an individual eruption, which are labelled down the left-hand side and shown using colour: **(a, f, l)** Tarawera, **(b, g, m)** Rotokawau, **(c, h, n)** Rotomakariri, **(d, i, o)** Terrace Rd, and **(e, j, p)** other OVC basalts, which includes Kaharoa, Rerewhakaaitu, Okareka, and Matahi. The final row shows: **(k)** pyroxene Cr_2O_3 against Mg# and **(q)** feldspar FeO_T against An with symbols as in **(l)**. Symbol shape indicates analysis of grain or inclusion and unfilled symbols are data from profiles across grains. The different mineral types described in the text are indicated above panels: **(f)** for clinopyroxene (1, 2, and 3 in grey) and orthopyroxene (1 and 2 in white), and **(l)** for plagioclase (1, 2, and 3 in grey). *Abbreviations:* ol = olivine, cpx = clinopyroxene, opx = orthopyroxene, fsp = feldspar, xst = crystal, and μlite = microlite. *Data references:* Matahi (Davis, 1985), Terrace Rd (Law et al., 2021; this study), Rotomakariri (Law et al., 2021; this study), Okareka (Barker et al., 2020; Shane et al., 2008a), Rerewhakaaitu (Shane et al., 2007), Rotokawau (Beanland, 1989; Hiess et al., 2007; Law et al., 2021; this study), Kaharoa (Barker et al., 2020; Leonard et al., 2002), and Tarawera (Barker et al., 2020; Hiess et al., 2007; Law et al., 2021; Rowe et al., 2021; this study).

There are broadly three types of clinopyroxene (Figure 3f–k). Type one has high Mg# (>83) and is found at Tarawera with low Cr_2O_3 (<1500 ppm) and Rotomakariri and Terrace Rd with high Cr_2O_3 (>2000 ppm). Type two has Mg# 78–83 and occurs at Rotokawau and Terrace Rd. Type three has Mg# 67–81 and occurs in Rotomakariri, Rotokawau and rarely in Tarawera (including groundmass clinopyroxene reported by Rowe et al. (2021) for Tarawera). At Rotomakariri, clinopyroxene grains are 100–500 μm in size; smaller grains are largely unzoned but larger grains have faint oscillatory zoning. The rims always show evidence of partial resorption and sometimes a thin band of coarse sieving occurs just before the outermost rim. At Rotokawau, clinopyroxene crystals are unzoned or weakly oscillatory-zoned.

Orthopyroxene is only common in Rotomakariri, occurring as two types (Figure 3f–k). Type one is high Mg# (65–80) and is found as macrocrysts in Rotomakariri (and rarely Rotokawau and Tarawera) and sometimes occurs as inclusions in lower Mg# clinopyroxene grains at Terrace Rd and Rotokawau. Type two is low Mg# (46–57), sometimes contains inclusions of apatite, and is found in all eruptions. At Rotomakariri, orthopyroxene (100–500 μm) is mostly unzoned, but always contains a fine band of sieving just before the rim. At Terrace Rd, a broken fragment of a much larger orthopyroxene crystal displays a newly crystallised clinopyroxene rim.

Plagioclase is present in three populations (Figure 3l–q). Type one plagioclase is large (250–500 μm, but up to 1 mm in size), mostly equant (although at Terrace Rd the aspect ratio is 2–3), and found in all eruptions. Type one cores are very calcic (>An_{90}) with coarse sieving and normally zone to a thin, unsieved, less calcic rim ($An_{83–88}$, occasionally to An_{80} at Tarawera). Type two plagioclase is typically smaller (<250 μm), lath-shaped (e.g., aspect ratios >4 for Terrace Rd), and mostly unzoned ($An_{82–87}$, occasionally An_{55}). At Rotomakariri, type two plagioclases are often fragmented. They also occur as inclusions in clinopyroxene at Terrace Rd, in low Mg# orthopyroxene at Rotokawau, and in both clinopyroxene and orthopyroxene at Rotomakariri. This composition is similar to the rims on type one plagioclase and the plagioclase microlites in the groundmass measured by Rowe et al. (2021) for Tarawera. For both type one and type two plagioclase FeO content is high (>0.4 wt%) and decreases with increasing anorthite (Figure 3e). Type three plagioclase is large (250–1000 μm), low in anorthite ($An_{22–53}$) and FeO (<0.4 wt%), and texturally variable (Figure 3e). At Terrace Rd, type three plagioclases are lath-shaped, have rounded edges, a distinct core with oscillatory overgrowth, and sometimes occur in xenoliths of high-silica, fluidal groundmass (Figure 2p).

At Rotomakariri the majority of the plagioclase grains (~75 area%) are type three, which are large (mostly 0.5–2 mm, up to 2.5 mm in size) and tabular in shape (extinction angle on twins suggests $An_{\sim 55}$). Crystals are oscillatory zoned, often display pervasive coarse sieving, and are weakly normal-zoned to the rims. At Rotokawau, these plagioclase grains have either coarsely sieved cores or show no internal texture but have weak oscillatory zoning and partial resorption at the edges. At Tarawera they are homogeneous and unzoned, with some dissolution at the rim.

Glomerocrysts are common at Terrace Rd, Rotokawau, and Rotomakariri (Figure 2i–n). Unlike mineral types, which were shared across different eruptions (e.g., type one plagioclase or type two clinopyroxene), glomerocryst types are unique to individual eruptions, and are therefore labelled with reference to the host eruption. There are three types of glomerocrysts at Terrace Road (Tr): type Tr-A comprises multiple type one plagioclase crystals often occurring with a synneusis of small olivine grains around the edge (Figure 2e); type Tr-B comprises small crystal clots (<500 μm in size) of lath-shaped type two plagioclase growing from a central olivine with abundant clinopyroxene (Figure 2i); and type Tr-C contains large, reversely-zoned clinopyroxene (>500 μm in size; Mg# = 66 core, 80 mid-to-rim zone), type one plagioclase, and minor olivine (Figure 2**Error! Reference source not found.**m). At Rotokawau clinopyroxene sometimes occurs in small glomerocrysts with type two plagioclase (<400 μm in size) (Figure 2k). At Rotomakariri (Rm), a significant proportion of the crystal content is hosted in two types of glomerocrysts. Type Rm-A glomerocysts (2–3 mm across) contain 1–3 olivine nuclei (each 200–1000 μm in size) that are overgrown and/or joined by anhedral orthopyroxene (up to 500 μm in size) and minor clinopyroxene (up to 250 μm in size) (Figure 2n). In some cases, Rm-A glomerocysts are mantled by equal proportions of clinopyroxene, orthopyroxene, and plagioclase (similar to type one), which have euhedral faces and are 250–500 μm in size. Type Rm-B glomerocrysts (1–2 mm across) contain type three clinopyroxene, type one orthopyroxene, and type two plagioclase, with individual grains up 500 μm in size (Figure 2j). Plagioclase grains are diffusely normal-zoned with distinct clear, rims ($An_{83–79}$); pyroxenes can be weakly reverse-zoned when in contact with groundmass.

4.2 Melt inclusions

The vast majority of glass analyses in this study come from melt inclusions hosted in clinopyroxene, with minor analyses of olivine-, plagioclase-, and orthopyroxene-hosted melt inclusions, and groundmass glasses (Figure 4). Melt inclusions show considerable range in composition. Terrace Rd, Rotokawau, and Tarawera melt inclusions are predominantly basaltic to basaltic-andesite in composition, whereas Rotomakariri glasses are entirely dacitic. The Tarawera dataset is supplemented with melt inclusion data from Barker et al. (2020) and Rowe et al. (2021).

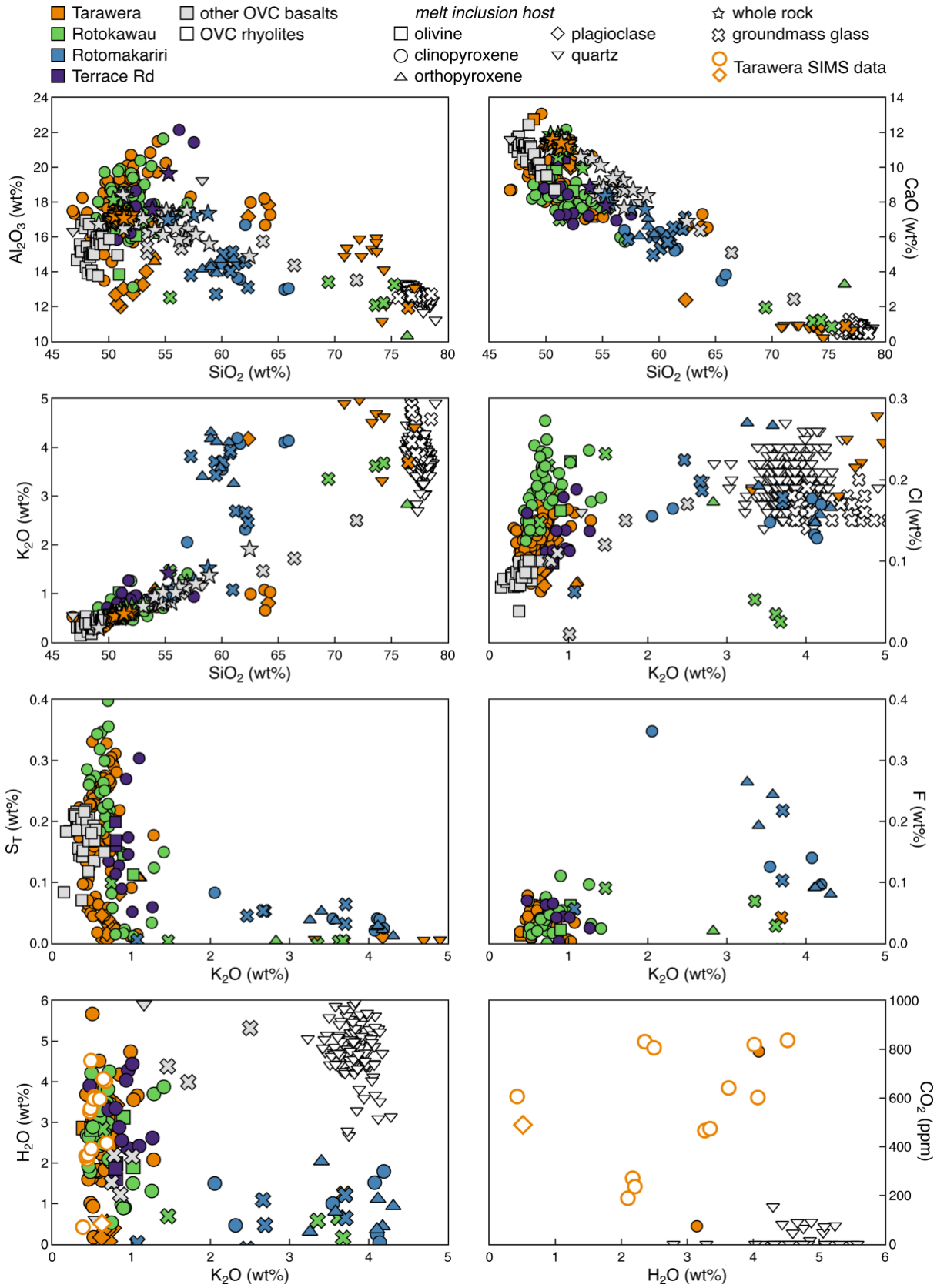

Figure 4 Melt inclusions (in olivine, clinopyroxene, plagioclase, orthopyroxene, or quartz, as indicated by symbol shape), groundmass glass, and whole rock data for OVC basalts (indicated by symbol colour – grey data are for Kaharoa, Rerewhakaaitu, Okareka, and Matahi) and rhyolites (white). Melt inclusion data are raw analyses (i.e., no corrections for post-entrapment processes), except Kaharoa, Okareka and three olivine-hosted Tarawera melt inclusions that

were homogenised prior to measurement by Barker et al. (2020). All data from this study are from EPMA, except open symbols outlined in orange that are SIMS data. *Data references:* melt inclusion and groundmass glass for Terrace Road, Rotomakariri, and Rotokawau (this study); Tarawera melt inclusions hosted in clinopyroxene and plagioclase (this study; Rowe et al., 2021), olivine (Barker et al., 2020), orthopyroxene and quartz (Rowe et al., 2021); olivine-hosted melt inclusions for Okareka and Kaharoa (Barker et al., 2020); glass analyses from mafic blebs from Rerewhakaaitu (Shane et al., 2007); melt inclusions and groundmass glass from OVC rhyolites (Johnson et al., 2011); and OVC basaltic whole rock (Beanland, 1989; Bowyer, 2001; Cole, 1979, 1973b; Gamble et al., 1993, 1990; Grange, 1937; Hiess et al., 2007; Leonard et al., 2002; Nairn, 1992, 1981, 1979; Nairn et al., 2004; Nairn, 2002; Pittari et al., 2016; Rooney and Deering, 2014; Rowe et al., 2021; Schmitz and Smith, 2004; Shane et al., 2008a; Zellmer et al., 2020). Additional oxides are shown in Supplementary Material.

Basaltic to basaltic-andesite melt inclusions are similar in type one and type two clinopyroxenes and olivines from Terrace Rd, Rotokawau, and Tarawera, although olivine-hosted melt inclusions at Terrace Rd have higher CaO. MgO correlates negatively with Al_2O_3 and positively with CaO, although some melt inclusions from Rotokawau deviate from this trend. There is no trend in melt chemistry with clinopyroxene Mg#, although the two melt inclusions hosted in Mg# 76 clinopyroxene have the most evolved melt chemistry at Rotokawau. At Rotokawau and Tarawera, these melt inclusions have a wide range in H_2O content (0–5.5 wt%), whereas H_2O concentrations at Terrace Rd have a more limited range (2.2–4.8 wt% H_2O) (Figure 4). Terrace Rd and Tarawera have similar chlorine concentrations (1110–1880 and 630–1870 ppm Cl, respectively) that are lower than Rotokawau (1250–2730 ppm Cl). Total sulphur (S_T) has a similarly wide range in all three eruptions (50–3980 ppm S_T) and fluorine concentrations are also similar (290–1100 ppm F). CO_2 was only measured for a subset of Tarawera melt inclusions (74–831 ppm CO_2). Broadly, there is a negative correlation of MgO with H_2O, S_T and Cl, and a positive correlation for K_2O (Figure 4). At Rotokawau and Tarawera, there is a second population of melt inclusions with S_T <1000 ppm where H_2O and S_T (but not Cl) positively correlate with MgO (and negatively correlate with K_2O). Tarawera melt inclusions hosted in type one plagioclase are basaltic with either the same (single grain) or higher MgO, lower Al_2O_3, and volatile-poor in comparison to clinopyroxene-hosted melt inclusions, where MgO, S_T, and Cl correlate positively (single grain from this study). The basaltic-andesite inclusions hosted in orthopyroxene have similar CaO, but different Al_2O_3, to clinopyroxene-hosted melt inclusions (Rowe et al., 2021).

Rotomakariri melt inclusions hosted in type three clinopyroxene and type two orthopyroxene and groundmass glass are dacitic, with low MgO and Al_2O_3 that positively correlate (Figure 4). H_2O and S_T are lower than most of the basaltic to basaltic-andesite melt inclusions, although similar to the low-sulfur (S_T <1000 ppm) set of clinopyroxene-hosted melt inclusions. Chlorine is high and similar to Rotokawau and fluorine is much higher than any of the basalts. At Tarawera, a few clinopyroxene-hosted melt inclusions are also dacitic, but have higher Al_2O_3 and lower K_2O than Rotomakariri melt inclusions. A single dacitic melt inclusion hosted in an Na-rich plagioclase from Tarawera has similar Al_2O_3 to the other Tarawera dacitic melt inclusions, but similar K_2O to the Rotomakariri dacitic melt inclusions. Rhyolitic melt inclusions and groundmass glass are associated with type two orthopyroxene and quartz from Rotokawau and Tarawera and have very low S_T (0–70 ppm).

Crystallisation, diffusion, and bubble-formation can alter major and volatile element chemistry of melt inclusions after entrapment (e.g., Barth et al., 2019; Barth and Plank, 2021; Bucholz et al., 2013; Danyushevsky et al., 2000, 1988; Dungan and Rhodes, 1978; Gaetani et al., 2012; Gaetani and Watson, 2002, 2000; Hartley et al., 2014, 2015; Lowenstern, 2003, 1995; Moore et al., 2015; Nielsen et al., 1998; Rasmussen et al., 2020; Roedder, 1979; Saper and Stolper,

2020; Schiano, 2003; Sobolev and Shimizu, 1993; Wallace et al., 2015). However, even when assuming the maximum degree of post-entrapment crystallisation (without Mg-Fe diffusion) for each melt inclusion, *trends* in major and volatile element chemistry do not change from those observed using the raw data (details in Supplementary Material). Hence, these trends reflect pre-entrapment processes for major elements. For this reason, uncorrected (i.e., raw) melt inclusion compositions are used throughout (Figure 4). Only the glass composition of melt inclusions was analysed; there was no attempt to account for volatiles contained in co-existing vapour bubbles (i.e., composition and size of vapour bubbles were not measured) to reconstruct bulk melt inclusion compositions. Thus, glass compositions represent minimum estimates of total melt inclusion volatile contents, as some portion may reside in the bubble (e.g., Hartley et al., 2014; Maclennan, 2017; Moore et al., 2015; Rasmussen et al., 2020; Wallace et al., 2015). CO_2 is greatly affected by bubble formation, whilst H_2O, S, and Cl are less affected due to lower partitioning into the vapour phase and potential kinetic effects (e.g., Rasmussen et al., 2020). Bulk (i.e., melt + bubble) H_2O content can additionally be altered by diffusion into or out of the melt inclusion (e.g., Barth et al., 2019; Barth and Plank, 2021; Bucholz et al., 2013; Gaetani et al., 2012; Hartley et al., 2015, 2014). Although we use raw volatile data, interpretations take into account the potential effects of bubble formation and de/rehydration.

5 Pre- and syn-eruptive storage, evolution, and mixing of multiple magmas

The bulk magma (i.e., whole rock) composition erupted in OVC basaltic eruptions (and found as basaltic enclaves in rhyolitic eruptions) is similar (Figure 4). However, the different compositional types of clinopyroxene, orthopyroxene, and plagioclase, in combination with different melt inclusion compositions, indicate that multiple magma types are found across these basaltic eruptions (Figure 3 and Figure 4). Therefore, it is useful to group these magma types when discussing magmatic evolution during crustal storage. Based on the mineral and melt inclusion compositions there are five different magma types. There are two basaltic to basaltic-andesite magmas found in all eruptions (Basalt-1 and Basalt-2); two dacitic magmas that are much less common and more specific to the Rotomakariri (Rm) and Tarawera (Tw) eruptions (Dacite-Rm and Dacite-Tw); and a minor amount of rhyolitic magma found in all eruptions. These magma types are repeatedly sampled as the groups of mineral types and melt inclusion compositions are common to many different eruptions. Similar melt inclusions (albeit more primitive) and mineral chemistries are found in other OVC basalts (e.g., Kaharoa, Okareka, Matahi, and Matahina) and even Taupō Volcanic Centre (TVC) basaltic material (e.g., Oraunui), showing these are common features within the TVZ (Allan et al., 2017; Barker et al., 2020; Deering et al., 2011; Rooyakkers et al., 2018; Wilson et al., 2006). Each magma type reflects differences in source (e.g., initial magma composition due to degree of slab influence), storage conditions (e.g., pressure, temperature, oxygen fugacity), processes (e.g., varying degrees of cooling- or decompression-induced crystallisation or crustal assimilation), or combinations thereof. As the same magma types occur in eruptions separated spatially and temporally, these sets of conditions must be common in the OVC (and potentially TVZ calderas more generally) even though magmas were not sourced from the same spatio-temporal reservoir.

We use oxy-thermo-barometry (calculation details are in Supplementary Material) and comparison to experiments to explore the conditions for Basalt-1, Basalt-2, and Dacite-Rm. The textures observed in each eruption reflect different interactions during ascent, such as magma mixing and microlite crystallisation. We compare the storage conditions and extents of mixing for magmas feeding basaltic eruptions with differing eruption styles.

5.1 Basalt-1

Basalt-1 encompasses most of the mineral and melt inclusion analyses in this study, namely type one and two clinopyroxene, type two plagioclase, and their melt inclusions; and the groundmass material (except for Rotomakariri) (Figure 3 and Figure 4). Olivine compositions show these are not primary mantle-derived melts and therefore these melts have already undergone crystallisation deeper in the system (Law et al., 2021). Both group one and two olivines as defined by Law et al. (2021) could have been derived from Basalt-1, where group two olivines crystallised deeper in the system and are sourced from cumulates. Alternatively, group two olivines may require a separate basaltic melt. The more primitive melt inclusions in this group have elevated volatile concentrations, reflecting the influence of a subducted slab component added to the mantle wedge source regions (e.g., Wysoczanski et al., 2006). The more evolved (but still basaltic-andesite) melt inclusions have even higher volatile concentrations, which are similar to (H_2O, Cl) or greatly exceed (CO_2, S_T) volatile concentrations in OVC rhyolites (e.g., Johnson et al., 2011). This supports the inference that basalts exchange volatiles with rhyolitic magmas during crustal interactions (e.g., Leonard et al., 2002; Shane et al., 2008a, 2008b, 2007). Additionally, Basalt-1 at Rotokawau has higher S_T and Cl concentrations compared to the other basaltic eruptions (Figure 4). For Tarawera and Rotokawau, melt inclusions can be divided into two sub-groups based on S_T concentrations above and below ~1000 ppm (Figure 4).

The spread in temperatures inferred from thermometry suggests cooling-induced crystallisation is responsible for the compositional range of whole rock and melt inclusion data (Figure 5a). The narrower spread in compositions and temperatures for whole rock and minerals compared to melt inclusions is broadly controlled by the basaltic bulk composition of the system. Conversely, melt inclusion compositions reflect changes in temperature and associated crystallisation, recording the melt present in the primary mush system near the solidus. The mushy nature of storage is also evidenced by abundant glomerocrysts in Terrace Rd, Rotomakariri, and Rotokawau (Figure 2i–n). A wide range of pressures (~700 MPa to surface) is derived from melt-clinopyroxene barometry, with most estimates <300 MPa (Figure 5b). The highest H_2O-CO_2 measurements require some melts to be derived from at least 400 MPa (Figure 5b). These estimates overlap with pressure-temperature estimates for Tarawera from Rowe et al. (2021), and imply polybaric storage of basaltic magmas. The limited literature whole rock Fe^{3+}/Fe_T data imply relatively oxidised conditions (~ΔNNO+1). Despite broadly similar melt chemistry between eruptions, the detailed mineral compositions (e.g., olivine and clinopyroxene, Figure 3) and glomerocryst textures are distinct (Figure 2i–n) indicating evolution in discrete, isolated pods prior to eruption, consistent with the temporal and spatial spread of eruptions.

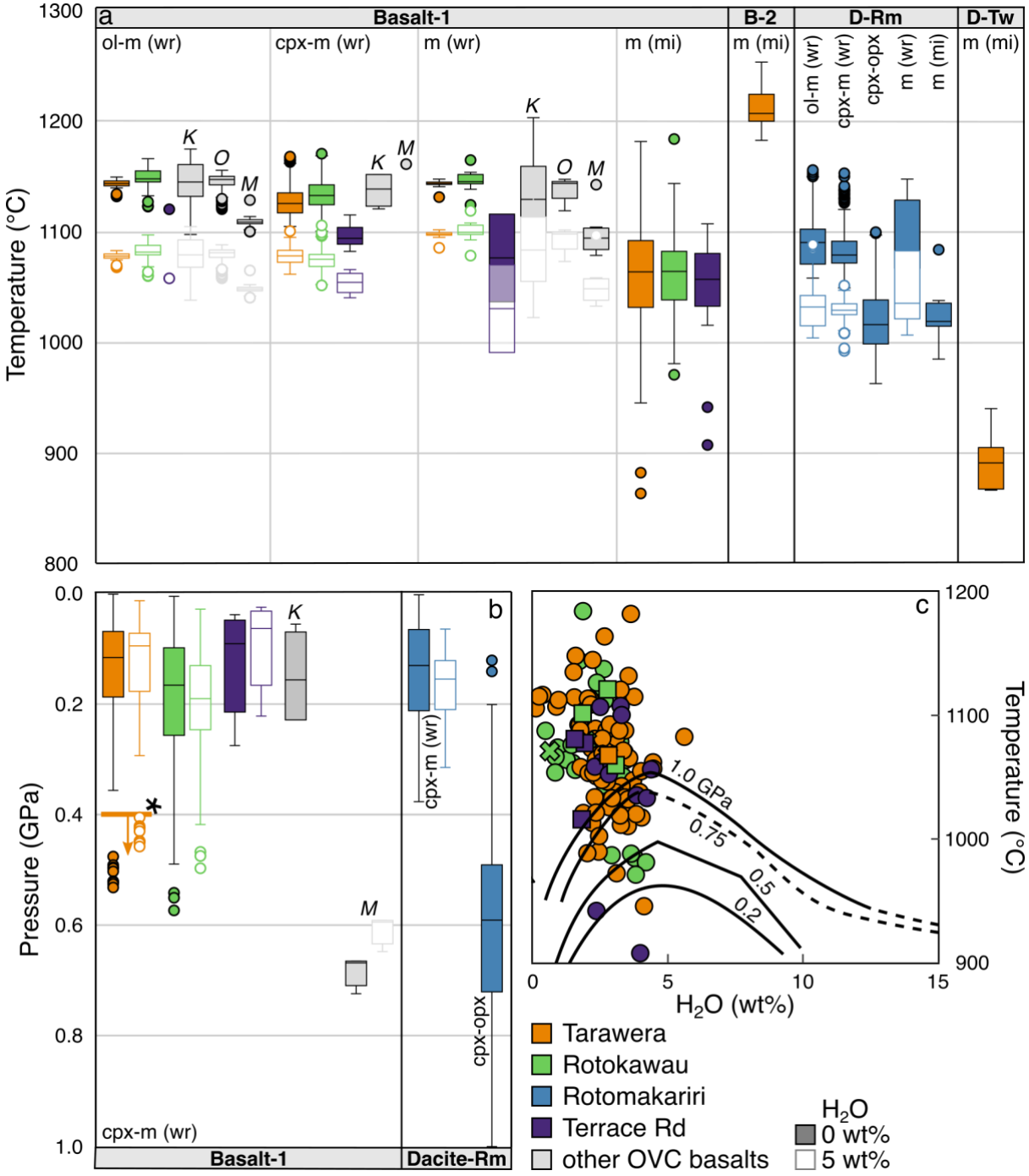

Figure 5 Box and whisker plots for **(a)** temperature and **(b)** pressure for each eruption (shown by colour – other OVC basalts include Kaharoa, Okareka, and Matahi, specified by a letter) grouped by magma type in **bold** (along the top of (a) and the bottom of (b)) and then by method. The edges of the "box" are at the 1st and 3rd quartile of the data, with the median indicated by a horizontal line within the box. The "whiskers" extend out to the minimum and maximum data points within 1.5× the interquartile range (range between 1st and 2nd quartile) beyond the 1st and 3rd quartiles. Any outliers outside the whiskers are shown as individual data points (circles). Estimates using whole rock compositions are shown assuming an anhydrous melt composition (filled) and H_2O-saturated up to 5 wt% (unfilled), whereas the measured H_2O content is used for melt inclusions. A minimum pressure estimate (indicated by a horizontal line (*) and a downwards pointing arrow) using the highest H_2O-CO_2 melt measurement is shown for Tarawera. *Abbreviations*: ol = olivine, m = melt, wr = whole rock, cpx = clinopyroxene, mi =

melt inclusion, opx = orthopyroxene, B-2 = Basalt-2, D-Rm = Dacite-Rm, D-Tw = Dacite-Tw, K = Kaharoa, O = Okareka, and M = Matahi. Full descriptions of the calculations are given in Supplementary Material. **(c)** Temperature against H_2O content. Lines are the maximum temperature amphibole is stable at for a given bulk H_2O content of the system from Foden and Green (1992) for different pressures (written on each line). Symbols (see Figure 4 for interpretation of the symbol shape) are melt inclusion data, where temperature is derived from the melt inclusion composition and the measured H_2O concentration is plotted, which is a minimum for the system.

Trends for H_2O and CO_2 are scattered, reflecting post-entrapment processes overprinting primary magmatic conditions, such as bubble formation reducing CO_2 concentrations and H-diffusion modifying H_2O (e.g., Barth et al., 2019; Barth and Plank, 2021; Bucholz et al., 2013; Gaetani et al., 2012; Hartley et al., 2015, 2014; Maclennan, 2017; Moore et al., 2015; Rasmussen et al., 2020; Wallace et al., 2015) (Figure 4). The highest measured concentrations are ~5 wt% H_2O and ~800 ppm CO_2, reflecting lower bounds on the maximum H_2O-CO_2 concentrations of the magma. The measured water contents overlap with inferred melt water contents from melt inclusions and clinopyroxene H contents from Rowe et al. (2021). A CO_2 content of 800 ppm would require at least 0.9 to 4.3 × 10^6 t/d (90 % confidence interval) of magma to degas fully to sustain the current levels of passive CO_2 emissions observed along the Tarawera fissure (Hughes et al., 2019b; Mazot et al., 2014). Positive correlation of Al_2O_3 and SiO_2 in clinopyroxene-hosted melt inclusions, reaching up to ~22 wt% Al_2O_3, requires plagioclase-suppression during crystallisation, such that clinopyroxene (± olivine) crystallisation controls melt composition (Figure 4). From experiments, attaining such high Al_2O_3 concentrations requires at least some crystallisation of an H_2O-rich magma at depth (e.g., Blatter et al., 2013; Müntener and Ulmer, 2018; Nandedkar et al., 2014). This is consistent with high H_2O contents (~5 wt%) measured in some melt inclusions and the high pressures from melt-clinopyroxene and melt H_2O-CO_2 barometry (Figure 5b).

Amphibole was not observed in the eruptions studied here; it has only been described in the groundmass of basaltic and gabbroic enclaves from the Kaharoa eruption (Leonard et al., 2002). At Kaharoa, amphibole crystallisation is thought to have been triggered by a late-stage increase in H_2O, possibly due to interaction with rhyolite (Leonard et al., 2002). Most of the melt inclusions at Tarawera, Rotokawau, and Terrace Rd record temperatures that are too high (>1050 °C) for amphibole stability despite their relatively high H_2O concentrations (Figure 5c) (Foden and Green, 1992). This suggests that basalt-rhyolite mixing prior to the Kaharoa eruption caused cooling of the basalt into the amphibole stability field, rather than increasing the H_2O content of the basalt.

Sulphur concentrations in melt inclusions require two separate regimes of crystallisation as previously observed by Rowe et al. (2021); we suggest these are isobaric cooling and decompression-induced degassing (Figure 4). Concentrations of S_T and Cl increase in the melt during crystallisation for melt inclusions with >1000 ppm S_T, indicating these volatiles behave incompatibly (i.e., not partitioned into coexisting solids or exsolved fluids) (Figure 4). The magma may have been volatile-undersaturated, and therefore there was no fluid phase for Cl or S to partition into, or fluid-melt partition coefficients for S and Cl were low (e.g., Gennaro et al., 2021; O'Neill, 2020; Tattitch et al., 2021; Thomas and Wood, 2021). If the magma was initially fluid-undersaturated, this would contrast with most arc regions where high magmatic CO_2 concentrations result in vapour-saturation deep in the crust (e.g., Wallace, 2005). Rotokawau and Tarawera melt inclusions with <1000 ppm S_T show the same trend for chlorine but the opposite trend for sulfur (i.e., decreasing S_T with crystallisation, Figure 4). Decreasing pressure during ascent drives crystallisation and degassing, forming a fluid that sequesters S, but not Cl (e.g., Lesne et al., 2011). The melt initially contained ~1700 ppm S_T and ~700 ppm

Cl (~1200 ppm Cl for Rotokawau), but the maximum concentrations are ~3000 ppm S_T and ~2000 ppm Cl (2800 ppm Cl for Rotokawau).

In summary, Basalt-1 is volatile-rich and evolved from a single, primitive, likely oxidised (~ΔNNO+1) magma in distinct, isolated, mushy pods due primarily to cooling-induced (1150 to 900 °C) crystallisation, and some degassing during ascent from pressures less than ~700 MPa.

5.2 Basalt-2

Basalt-2 is represented primarily by type one plagioclase and its melt inclusions that are chemically distinct from Basalt-1 (Figure 3 and Figure 4). The ubiquitous thin rims of type two plagioclase (part of Basalt-1) at the edge of type one plagioclases show that these two basalts are not in equilibrium (Figure 2e–h). Additionally, $^{87}Sr/^{86}Sr$ data for these high-An plagioclases are distinctly more radiogenic than the groundmass, supporting the suggestion that they are derived from a separate magma (Rowe et al., 2021). Type one plagioclase composition is not only found in OVC basaltic material since ~55 ka, but also in basaltic material from the ~26.5 ka TVC Oruanui eruption (Allan et al., 2017; Rooyakkers et al., 2018; Wilson et al., 2006) and the ~330 ka OVC post-caldera deposits after the Matahina eruption (Deering et al., 2011). The ubiquity of type one plagioclase in spatially and temporally separated OVC (and TVC) basalts requires common crystallisation conditions.

High anorthite plagioclase (>An_{90}) is indicative of hydrous conditions (e.g., Panjasawatwong et al., 1995; Takagi et al., 2005). Plagioclase-liquid hygrometry using Waters and Lange (2015) suggests 5–7 wt% H_2O in the melt, yet the melt inclusions are almost anhydrous (Figure 4). This suggests hydrogen loss from the melt inclusions via diffusion, either during storage in a low-H_2O melt or degassing during ascent (e.g., Hamada and Fujii, 2007). The higher temperatures compared to Basalt-1 (up to ~1250 °C) recorded by the melt inclusions would then reflect their low H_2O content due to dehydration (Figure 5a).

High-An plagioclases have not been reported in basaltic material erupted outside active caldera regions, suggesting their formation is linked to calderas. Active caldera regions are likely to have higher magmatic water contents (and hence produce high-An plagioclase) as melting is driven by fluid-fluxing of a fertile mantle (e.g., Barker et al., 2020; Zellmer et al., 2020). Their occurrence as inclusions in clinopyroxene indicates plagioclase crystallisation before clinopyroxene, suggesting shallow crystallisation conditions, although unfortunately no further constraints on pressure could be made. These plagioclase crystals are likely in equilibrium with the most primitive TVZ basalts (Wilson et al., 2006) and perhaps an external control in the shallow crust causes isolated pods of basalt to stall at this level, which favours the crystallisation of type one plagioclase. For instance, these melts may pond under rhyolitic-andesitic magma reservoirs (i.e., >100 MPa; e.g., Cole et al., 2014). Alternatively, they could be generated by partial melting of pre-existing gabbros (e.g., Koepke et al., 2004). In summary, Basalt-2 is hydrous and likely crystallises at shallow depths.

5.3 Evolved magmas: Dacite-Rm, Dacite-Tw, and Rhyolite

Dacite-Rm is the main magma type for the Rotomakariri eruption, containing type three clinopyroxene, type one orthopyroxene, their melt inclusions, and the groundmass material (Figure 3 and Figure 4). The occurrence of type three clinopyroxene in other eruptions suggests Dacite-Rm, although uncommon in the OVC, is not unique to Rotomakariri (Figure 3b). Two-pyroxene thermobarometry suggests high pressures (~600 MPa) and temperatures (~1000 °C) (Figure 5b). This is unusually hot for a dacite and could reflect resetting of the mineral

compositions when the dacitic magma interacted with Basalt-1 and Basalt-2. Rotomakariri melt inclusion H_2O contents are very low, but this could indicate diffusive loss of H_2O, which is supported by many Rotomakariri melt inclusions being crystallised (these were not analysed). The low Cl and S_T concentrations indicates partitioning into a coexisting fluid. This is expected at low pressures and the hot, dry melt conditions observed; especially for sulphur in more evolved melt compositions (e.g., Clemente et al., 2004; Gennaro et al., 2021; O'Neill, 2020; Tattitch et al., 2021; Thomas and Wood, 2021) (Figure 4).

Dacite-Tw is chemically distinct from Dacite-Rm and melt inclusions record a lower temperature of ~850 °C (pressures could not be estimated from the available data, Figure 5a). As evidence for Dacite-Tw is only found in a few melt inclusions at Tarawera, it is not considered volumetrically important in the OVC (Figure 4).

A rhyolitic magma type is found in all eruptions and is associated with type two orthopyroxene, type three plagioclase, quartz, alkali feldspars, and the rhyolitic melt inclusions (Figure 3 and Figure 4). It has a similar composition to magmas from OVC rhyolitic eruptions and is assumed to have evolved under similar conditions: pressures of 100–260 MPa from melt inclusion H_2O-CO_2 barometry, the presence of cummingtonite, and glass composition at or near to the quartz-albite-orthoclase-water ~200 MPa cotectic; and temperatures of 700–940 °C (narrower ranges are inferred for individual rhyolitic magma batches), mostly from Fe-Ti oxide thermometry and some from melt inclusion heating experiments (summarised in Cole et al., 2014; Smith et al., 2005).

5.4 Similar storage conditions and volatiles prior to eruptions of varying style

Basalt-1 is the main magma type present in OVC basaltic eruptions. It comprises most of the material at Tarawera, Rotokawau, and Terrace Rd, and this is also likely the case for Okareka and Matahi and the basaltic material from Kaharoa and Rerewhakaaitu (Figure 3 and Figure 4). Rotomakariri is an exception and is therefore excluded from the following discussion: it does contain Basalt-1 material but is mostly composed of Dacite-Rm (Figure 3 and Figure 4). Temperature estimates using various thermometers based on whole rock compositions from the different eruptions overlap (~1150 °C anhydrous or ~1090 °C assuming 5 wt% H_2O, Figure 5a). Terrace Rd and Matahi record lower temperatures by ~50 °C but these eruptions also have fewer data to average (Figure 5a). Temperature estimates from melt inclusions for Tarawera, Rotokawau, and Terrace Rd are similar (1040–1090 °C), although the temperature range is greater at Tarawera and smallest at Terrace Rd (Figure 5a and c). Except Matahi that records deeper pressures than the other eruptions (600–700 MPa), the magmas of these eruptions are mostly stored at 50–250 MPa, with evidence for magmas as deep as 600 MPa (Figure 5b). However, despite the similar pre-eruptive compositions and conditions of Basalt-1, there is a wide variation in eruption style, and therefore no systematic relationship between storage conditions and eruption style (Figure 1b and Figure 5). Bamber et al. (2019) suggested moderate storage temperatures (<1100 °C) are important for generating basaltic Plinian eruptions, which do characterise Tarawera, but are also found for the smaller intensity eruptions (Figure 5a).

Volatile concentrations (H_2O, Cl, and S) and degassing paths are also similar between OVC basaltic eruptions (Figure 4). High H_2O concentrations suggest H_2O exsolution was important during ascent, which may drive basaltic Plinian eruptions (Bamber et al., 2019; Pérez et al., 2020). However, high H_2O concentrations are found across the range of eruption styles and are therefore not unique to Tarawera (Figure 4 and Figure 5c). Both Rotokawau and Tarawera have a population of melt inclusions that display degassing trends, and this population may have

been missed at Terrace Rd where fewer melt inclusions were analysed. The unique degassing path for Plinian eruptions compared to other explosive eruptions proposed by Moretti et al. (2018) led to lower Cl but higher S in less explosive eruptions compared to more explosive eruptions due to the differences in dehydration and sulphide-saturation that occur during crystallisation. However, the observed differences in S_T and Cl concentration in the OVC do not relate to eruption style: Rotokawau has higher S_T and Cl but intermediate eruption intensity between Terrace Rd and Tarawera and there is no evidence for sulphide-saturation (Figure 4). High CO_2 concentrations are thought to be important for generating (sub-)Plinian basaltic eruptions (e.g., Allison et al., 2021; Sable et al., 2009), which could be important in the OVC. Unfortunately, our CO_2 data for Tarawera are likely compromised by bubble formation and we do not have sufficient data to compare against smaller eruptions.

External influences within the crust could also influence eruption style of OVC basaltic magmas. OVC basaltic eruptions are tectonically controlled, as evidenced by the linear nature of their eruptive vents underlain by dikes (Nairn and Cole, 1981). Hence, these eruptions may be triggered by earthquakes, especially given the high melt H_2O contents and mushy-nature of storage, which could also influence eruption style (e.g., Hamling and Kilgour, 2020; Seropian et al., 2021). Additionally, the presence and physical state (e.g., viscosity) of large silicic bodies in the crust could affect basaltic eruption style by impeding (or not) the ascent of basaltic magmas to the surface. The tectonics in addition to the complex nature of the crust below the OVC may therefore be important for generating the wide variety of basaltic eruption style observed in the region.

5.5 Magma mixing during ascent influenced by eruption style

The occurrence of multiple magma types within single eruptions requires mixing. This suggests isolated pods of basaltic and more silicic material evolve in the crust and are then assembled just prior to or during ascent and erupted at the surface (e.g., Cole et al., 2014; Leonard et al., 2002; Schmitz and Smith, 2004; Shane et al., 2008a, 2007). Textural evidence suggests variable extents of mixing between eruptions and short pre-eruptive timescales for mixing.

Firstly, there is evidence for the mixing of multiple basaltic magmas. Textures in the scoria are indicative of mixing between different batches of Basalt-1 and Basalt-2 that have subtly different crystallisation conditions (i.e., come from different places in the magmatic system) or decompression histories (e.g., T–H_2O conditions). At Tarawera, there are multiple instances of Basalt-1, including the carrier melt (as represented by the macrocryst-poor whole rock composition), and the low/high-S_T melt inclusions (Figure 4). A similar picture applies to Rotokawau, where mingled groundmass textures suggest multiple carrier melts from Basalt-1 (Figure 2c). For Terrace Rd, the small type Tr-B glomerocrysts could be phenocrystic or antecrystic, whereas the large type Tr-C glomerocrysts, as well as the large orthopyroxene crystals (Figure 2e, i, and m), are antecrystic. It is not clear whether all the antecrystic material came from the same place or event and how much melt was transported with the mixing event, although there is evidence for multiple melts in the groundmass. Additionally, all eruptions have antecrystic type one plagioclase from Basalt-2, with disequilibrium cores (coarse sieve textures) and a rim in equilibrium with the groundmass (Figure 2e–h). In all cases, the implication is that a carrier magma interacted with multiple different basaltic magma bodies as it ascended through the crust, picking up crystals *en route*. This is also seen in differences in oxygen isotopes compositions between crystals and groundmass in these eruptions (Law et al., *in review*). The timescales of these interactions were likely very short (e.g., to preserve multiple groundmass textures and produce the sharp rims of type two plagioclase around type one plagioclase, Figure 2c and e–h), and probably occurred during pre-eruptive magma ascent. The

extent of mixing is correlated with eruption style. Lower intensity eruptions (Terrace Road, Rotokawau) contain a high proportion of macro-crystals, whereas Tarawera has a negligible crystal cargo (0.5 vol%, Sable et al., 2009). As crystals were entrained during ascent, the carrier melt entrained more crystals as it passed through the mushes for the smaller eruptions than the Plinian eruption. This difference likely reflects the faster ascent rate of Plinian magmas, rather than the cause *per se* of varying eruption style.

Rotomakariri shows the most extreme evidence for mixing: a basaltic crystal cargo with little basaltic melt mobilisation (from Basalt-1 and Basalt-2) is found in dacitic magma (Dacite-Rm) (Figure 2b, f, j, and n, Figure 3, and Figure 4). The crystal cargo consists mostly of large type Rm-A glomerocrysts, which may represent different segments of the same evolution sequence: olivine; orthopyroxene ± clinopyroxene; clinopyroxene + orthopyroxene + plagioclase (Figure 2f, j, and n). These glomerocrysts were rapidly mobilised during ascent, as the rims surrounding the antecrystic material are thin (Figure 2f, j, and n).

All four studied eruptions additionally show mixing with rhyolitic material (Figure 3 and Figure 4). At Terrace Rd and Tarawera, the rhyolitic material appears to have been incorporated at a late-stage of magma ascent (e.g., sharp boundaries between basaltic and rhyolitic material, Figure 2p), probably when the basaltic magma punched through previously erupted, cold residual rhyolite domes. Rotokawau shows evidence of both early- and late-stage rhyolitic mixing. Some incorporated plagioclase grains have pervasive resorption textures, suggesting basalt-rhyolite interaction, whereas the rhyolite was still hot and mushy. Conversely, other grains only show disequilibrium textures on the outermost edge suggesting incorporation from a cooler rhyolite. The other extreme is the Kaharoa eruption (and Rerewhakaaitu), where basaltic material is a minor component of a rhyolitic eruption (e.g., Leonard et al., 2002; Shane et al., 2007). This may highlight that slow ascent prevents basalts punching directly through rhyolite magma bodies, instead triggering rhyolitic eruption.

This diversity of magma types and mixing dynamics sampled both in individual eruptions and across eruptions from the OVC reflects the interplay between basaltic magma ascent rates and the distribution, composition, and rheological state of magma bodies both vertically and horizontally. As mixing timescales appear to be short for the basalts that reach the surface, precursory signals to basaltic explosive eruptions could be limited, as suggested by the observations of the Tarawera 1886 C.E. eruption (Keam, 1988).

6 The magmatic architecture of the OVC

Combining the evidence from barometry and mixing textures suggests a crust full of individual magmatic bodies beneath the OVC, that are variously sampled during eruption (Figure 6). All the pressures derived from clinopyroxene-melt and H_2O-CO_2 barometery are within the TVZ crust assuming a crustal density of 2700 $kg \cdot m^{-3}$ and a Moho at 25–30 km or 700–800 MPa pressure (Bannister et al., 2004). This suggests that basaltic magmas, in addition to rhyolitic magmas, are stored and evolve polybarically within the crust. This agrees with current geochemical and geophysical constraints from previous Tarawera clinopyroxene barometry (100–300 MPa, with some >700 MPa, reported in Sable et al., 2009) and the presence of partial melt bodies at similar depths around the OVC, such as at 6–16 km using receiver functions (Bannister et al., 2004), 10–20 km (as shallow as 8 km beneath Waimungu) using magneto-telluric and electrical resistivity inversions (Heise et al., 2016, 2010), and 8–10 km from earthquake swarms attributed to a basaltic dike intrusion (Benson et al., 2021). Additionally, conceptual models based on petrological modelling have mafic sheets residing at 11–15 km, with some isolated pods found at 8–6 km depths (Cole et al., 2014; Deering et al., 2010). The

observations from basaltic eruptions in the OVC suggest the crust is characterised by many pods of magma that fall into five main categories (Basalt-1, Basalt-2, Dacite-Rm, Dacite-Tw, and Rhyolite), but each batch has its own distinct composition reflecting their individual histories.

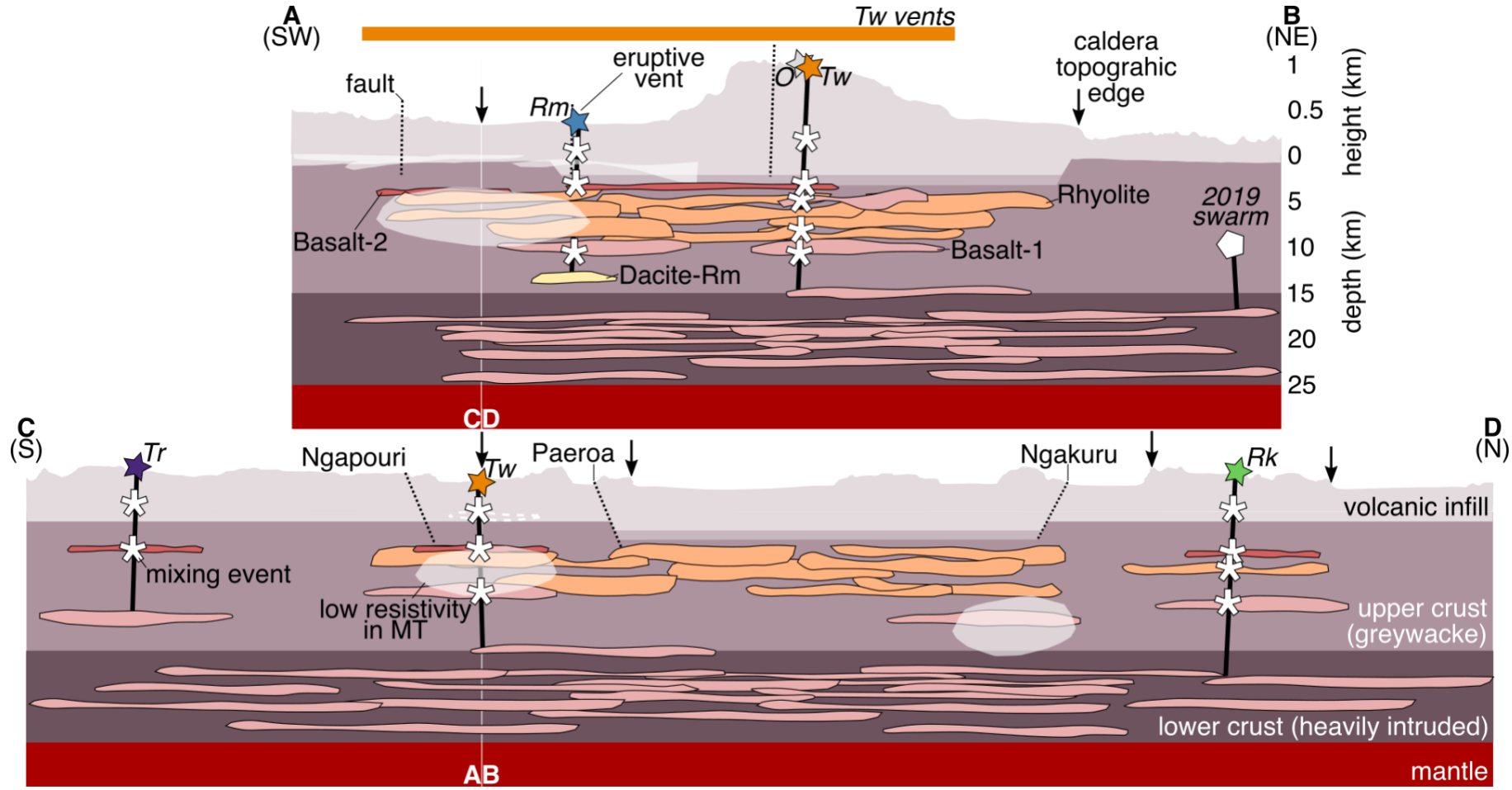
A
(SW)
Tw vents
B
(NE)
caldera
topograhic
edge
fault
eruptive
vent
Rm
O
Tw
1
0.5
0
5
10
15
20
25
height (km)
depth (km)
Rhyolite
2019
swarm
Basalt-2
Basalt-1
Dacite-Rm
CD
C
(S)
D
(N)
Tr
Ngapouri
Tw
Paeroa
Ngakuru
Rk
volcanic infill
mixing event
low resistivity
in MT
upper crust
(greywacke)
lower crust (heavily intruded)
mantle
AB

Figure 6 Schematic cross-sections showing the sub-surface magmatic architecture below the OVC integrated over the last ~55 ka. The upper section (AB) runs SW-NE along the fissure created by the 1886 C.E. Tarawera eruption and the lower section (CD) runs S-N, where the white vertical line in both represents where the two sections intersect (labelled AB and CD accordingly) and their locations are shown on Figure 1a. The vertical scales are the same in both sections (labelled on the upper section), but the height-scale is exaggerated compared to the depth-scale to show topographic features. The volcanic infill depth is taken from Seebeck et al. (2010) and the crust-mantle boundary from Bannister et al. (2004). The caldera topographic edge is indicated with a vertical arrow pointing down (Nairn, 2002) and faults are indicated with dotted black lines (and sometimes labelled – there locations are taken from Seebeck et al. (2010) and inferred from regions of high-CO_2 emissions from Hughes et al. (2019b)). Magmatic bodies are shown outlined in black, where the colour indicates the magma type: pink is Basalt-1, dark red is Basalt-2, yellow is Dacite-Rm, and orange is Rhyolite: their depths are based on this study and various other studies (Bannister et al., 2004; Cole et al., 2014; Heise et al., 2016, 2010; Johnson et al., 2011; Sable et al., 2009). The heavy-black lines indicate magma pathways to the surface to generate basaltic eruptions, where the white asterisks' indicate mixing events and the coloured stars at the surface show vent locations (the colour indicates the eruption as shown on Figure 1b and are labelled in *italics*: *Tw* = Tarawera, *Rk* = Rotokawau, *Rm* = Rotomakariri, *Tr* = Terrace Rd, and *O* = Okareka). As the upper section runs parallel to the Tarawera 1886 fissure only one vent is indicated but the orange horizontal bar represents the extent of the vents. The location of the 2019 earthquake swarm attributed to a basaltic dyke (Benson et al., 2021) is shown by a pentagon. The white transparent areas are low-resistivity regions images using magneto-telluric and electric resistivity surveys by Heise et al. (2016, 2010) – the whole region has not been surveyed so other low-resistivity regions likely exist.

These observations suggest that a thick, crustal mush – containing a wealth of magma types in individual, isolated pockets – is mostly trapping the ascending basalts that fuel magmatism in the OVC crust. This model likely applies to TVZ calderas more generally whilst active. This is similar to other arc settings, such as the Andean Puna plateau, resulting in the dominance of compositionally-evolved volcanism (e.g., Delph et al., 2017; Kay et al., 2010). However, the extensional regime of the TVZ is clearly important in allowing some of these basalts to reach the surface and erupt explosively. The few basalts that do make it to the surface have passed through the complicated crustal mush and carry the signature of these interactions in their crystal cargo. This highlights the use of basaltic mineral and melt inclusion chemistry as windows into the sub-surface in silicic magmatic regions, extending its application from using olivine-hosted melt inclusions to understand mantle melting dynamics (e.g., Barker et al., 2020), to additionally analysing clinopyroxene-hosted melt inclusions to gain insight into crustal processes. Combining data from multiple eruptions separated spatially and temporally has highlighted that similar processes are important across (and even beyond) the OVC for potentially the last ~30 ka.

7 Author Contributions

ECH, JDB, HMM, and GK conceived the project idea. ECH and SL collected and processed the data. All authors contributed to data interpretation. ECH led manuscript production with further contribution from all authors.

8 Acknowledgements

We would like to thank the Ruawahia 2B trust for welcoming us onto Mount Tarawera and permitting us to collect samples on the mountain and especially Ken Raureti, Tīpene Marr, and Paul Warbrick for their support of this work; Kaingaroa Timberlands for permits to access Kaingaroa Forest and Waimangu Forest to collect samples; Yves Feisel (now at the University of Mainz, Germany), Marco Michelini (now at the University of Pittsburgh, USA), Brad Scott (Te Pū Ao | GNS Science, Aotearoa New Zealand), Nick Macdonald (Te Pū Ao | GNS Science, Aotearoa New Zealand) for helping with basalt hunting; Richard Hinton for his assistance at the NERC ion microprobe facility at the University of Edinburgh, UK (IMF560/0515); and Stuart Kearns and Ben Buse for their assistance with the electron probe and SEM at the University of Bristol, UK. ECH was supported by a NERC GW4+ DTP studentship (NE/L002434/1) and is thankful for the support and additional funding from CASE partner Te Pū Ao | GNS Science, Aotearoa New Zealand, and a Geology Option Post-Doctoral Fellowship from Caltech, USA. SL was supported by a NERC E^3 DTP studentship (NE/L002558/1). GK is supported by the Hazards and Risk Management Programme, which is part of New Zealand Strategic Science Investment Funding (SSIF) from the New Zealand Ministry of Business, Innovation & Employment (MBIE). JDB acknowledges support through a Royal Society Professorship.

9 References

Allan, A.S.R., Barker, S.J., Millet, M.A., Morgan, D.J., Rooyakkers, S.M., Schipper, C.I., Wilson, C.J.N., 2017. A cascade of magmatic events during the assembly and eruption of a super-sized magma body. Contrib. to Mineral. Petrol. 172, 49. https://doi.org/10.1007/s00410-017-1367-8

Allison, C.M., Roggensack, K., Clarke, A.B., 2021. Highly explosive basaltic eruptions driven by CO2 exsolution. Nat. Commun. 12, 217. https://doi.org/10.1038/s41467-020-20354-2

Annen, C., Blundy, J.D., Sparks, R.S.J., 2006. The Genesis of Intermediate and Silicic Magmas in Deep Crustal Hot Zones. J. Petrol. 47, 505–539. https://doi.org/10.1093/petrology/egi084

Bamber, E.C., Arzilli, F., Polacci, M., Hartley, M.E., Fellowes, J., Di Genova, D., Chavarría, D., Saballos, J.A., Burton, M.R., 2019. Pre- and syn-eruptive conditions of a basaltic Plinian eruption at Masaya Volcano, Nicaragua: The Masaya Triple Layer (2.1 ka). J. Volcanol. Geotherm. Res. 106761. https://doi.org/10.1016/J.JVOLGEORES.2019.106761

Bannister, S.C., Bryan, C.J., Bibby, H.M., 2004. Shear wave velocity variation across the Taupo Volcanic Zone, New Zealand, from receiver function inversion. Geophys. J. Int. 159, 291–310. https://doi.org/10.1111/j.1365-246X.2004.02384.x

Barker, S.J., Rowe, M.C., Wilson, C.J.N., Gamble, J.A., Rooyakkers, S.M., Wysoczanski, R.J., Illsley-Kemp, F., Kenworthy, C.C., 2020. What lies beneath? Reconstructing the primitive magmas fueling voluminous silicic volcanism using olivine-hosted melt inclusions. Geology 48, 504–508. https://doi.org/10.1130/G47422.1

Barth, A., Newcombe, M., Plank, T., Gonnermann, H., Hajimirza, S., Soto, G.J., Saballos, A., Hauri, E., 2019. Magma decompression rate correlates with explosivity at basaltic volcanoes — Constraints from water diffusion in olivine. J. Volcanol. Geotherm. Res. 387, 106664. https://doi.org/10.1016/j.jvolgeores.2019.106664

Barth, A., Plank, T., 2021. The Ins and Outs of Water in Olivine-Hosted Melt Inclusions: Hygrometer vs. Speedometer. Front. Earth Sci. 9, 343. https://doi.org/10.3389/feart.2021.614004

Beanland, S., 1989. The Rotokawau Basalt. University of Otago.

Beanland, S., Houghton, B.F., 1978. Rotokawau Tephra : basaltic maars in Okataina Volcanic Centre, Taupo volcanic zone. New Zeal. Geol. Surv. Bull. 37–43.

Benson, T.W., Illsley-Kemp, F., Elms, H.C., Hamling, I.J., Savage, M.K., Wilson, C.J.N., Mestel, E.R.H., Barker, S.J., 2021. Earthquake Analysis Suggests Dyke Intrusion in 2019 Near Tarawera Volcano, New Zealand. Front. Earth Sci. 8, 604. https://doi.org/10.3389/feart.2020.606992

Blatter, D.L., Sisson, T.W., Hankins, W. Ben, 2013. Crystallization of oxidized, moderately hydrous arc basalt at mid- to lower-crustal pressures: implications for andesite genesis. Contrib. to Mineral. Petrol. 166, 861–886. https://doi.org/10.1007/s00410-013-0920-3

Bowyer, D.A., 2001. Petrologic, Geochemical and Isotopic Evolution of Rhyolite Lavas from the Okataina,

Rotorua and Kapenga Volcanic Centres, Taupo Volcanic Zone, New Zealand. University of Waikato.
Bucholz, C.E., Gaetani, G.A., Behn, M.D., Shimizu, N., 2013. Post-entrapment modification of volatiles and oxygen fugacity in olivine-hosted melt inclusions. Earth Planet. Sci. Lett. 374, 145–155. https://doi.org/10.1016/j.epsl.2013.05.033
Burt, R.M., Brown, S.J.A., Cole, J.W., Shelley, D., Waight, T.E., 1998. Glass-bearing plutonic fragments from ignimbrites of the Okataina caldera complex, Taupo Volcanic Zone, New Zealand: remnants of a partially molten intrusion associated with preceding eruptions. J. Volcanol. Geotherm. Res. 84, 209–237. https://doi.org/10.1016/S0377-0273(98)00039-0
Carey, R.J., Houghton, B.F., Sable, J.E., Wilson, C.J.N., 2007. Contrasting grain size and componentry in complex proximal deposits of the 1886 Tarawera basaltic Plinian eruption. Bull. Volcanol. 69, 903–926. https://doi.org/10.1007/s00445-007-0117-6
Clemente, B., SCAILLET, B., PICHAVANT, M., 2004. The Solubility of Sulphur in Hydrous Rhyolitic Melts. J. Petrol. 45, 2171–2196. https://doi.org/10.1093/petrology/egh052
Cole, J.W., 1979. Structure, petrology, and genesis of Cenozoic volcanism, Taupo Volcanic Zone, New Zealand—a review. New Zeal. J. Geol. Geophys. 22, 631–657. https://doi.org/10.1080/00288306.1979.10424173
Cole, J.W., 1973a. High-alumina basalts of Taupo Volcanic Zone, New Zealand. Lithos 6, 53–64. https://doi.org/10.1016/0024-4937(73)90079-0
Cole, J.W., 1973b. High-alumina basalts of Taupo Volcanic Zone, New Zealand. LITHOS 6, 53–64. https://doi.org/10.1016/0024-4937(73)90079-0
Cole, J.W., 1970a. Structure and eruptive history of the Tarawera Volcanic Complex. New Zeal. J. Geol. Geophys. 13, 879–902. https://doi.org/10.1080/00288306.1970.10418208
Cole, J.W., 1970b. Petrology of the basic rocks of the Tarawera Volcanic Complex. New Zeal. J. Geol. Geophys. 13, 925–936. https://doi.org/10.1080/00288306.1970.10418210
Cole, J.W., Deering, C.D., Burt, R.M., Sewell, S., Shane, P.A., Matthews, N.E., 2014. Okataina Volcanic Centre, Taupo Volcanic Zone, New Zealand: A review of volcanism and synchronous pluton development in an active, dominantly silicic caldera system. Earth-Science Rev. 128, 1–17. https://doi.org/10.1016/j.earscirev.2013.10.008
Coltelli, M., Del Carlo, P., Vezzoli, L., 1998. Discovery of a Plinian basaltic eruption of Roman age at Etna volcano, Italy. Geology 26, 1095. https://doi.org/10.1130/0091-7613(1998)026<1095:DOAPBE>2.3.CO;2
Danyushevsky, L., Della-Pasqua, F.N., Sokolov, S., 2000. Re-equilibration of melt inclusions trapped by magnesian olivine phenocrysts from subduction-related magmas: Petrological implications. Contrib. to Mineral. Petrol. 138, 68–83. https://doi.org/10.1007/PL00007664
Danyushevsky, L., Sobolev, A.V., Dmitriev, L.V., 1988. Orthopyroxene-bearing low-Ti tholeiites: The new type of ceanic ridge tholeiite. Trans. USSR Acad. Sci. Earth Sci. Sect. 292, 102–105.
Darragh, M.B., Cole, J.W., Nairn, I.A., Shane, P.A., 2006. Pyroclastic stratigraphy and eruption dynamics of the 21.9 ka Okareka and 17.6 ka Rerewhakaaitu eruption episodes from Tarawera Volcano, Okataina Volcanic Centre, New Zealand. New Zeal. J. Geol. Geophys. 49, 309–328. https://doi.org/10.1080/00288306.2006.9515170
Davis, W.J., 1985. Geochemistry and petrology of the Rotoiti and Earthquake Flat pyroclastic deposits. University of Auckland.
Deering, C.D., Cole, J.W., Vogel, T.A., 2011. Extraction of crystal-poor rhyolite from a hornblende-bearing intermediate mush: A case study of the caldera-forming Matahina eruption, Okataina volcanic complex. Contrib. to Mineral. Petrol. 161, 129–151. https://doi.org/10.1007/s00410-010-0524-0
Deering, C.D., Gravley, D.M., Vogel, T.A., Cole, J.W., Leonard, G.S., 2010. Origins of cold-wet-oxidizing to hot-dry-reducing rhyolite magma cycles and distribution in the Taupo Volcanic Zone, New Zealand. Contrib. to Mineral. Petrol. 160, 609–629. https://doi.org/10.1007/s00410-010-0496-0
Delph, J.R., Ward, K.M., Zandt, G., Ducea, M.N., Beck, S.L., 2017. Imaging a magma plumbing system from MASH zone to magma reservoir. Earth Planet. Sci. Lett. 457, 313–324. https://doi.org/10.1016/J.EPSL.2016.10.008
Ducea, M.N., Saleeby, J.B., Bergantz, G., 2015. The Architecture, Chemistry, and Evolution of Continental Magmatic Arcs. http://dx.doi.org/10.1146/annurev-earth-060614-105049 43, 299–331. https://doi.org/10.1146/ANNUREV-EARTH-060614-105049
Dungan, M.A., Rhodes, J.M., 1978. Residual glasses and melt inclusions in basalts from DSDP Legs 45 and 46: Evidence for magma mixing. Contrib. to Mineral. Petrol. 67, 417–431. https://doi.org/10.1007/BF00383301
Foden, J.D., Green, D.H., 1992. Possible role of amphibole in the origin of andesite: some experimental and natural evidence. Contrib. to Mineral. Petrol. 109, 479–493. https://doi.org/10.1007/BF00306551
Froggatt, P.C., Lowe, D.J., 1990. A review of late Quaternary silicic and some other tephra formations from New Zealand: Their stratigraphy, nomenclature, distribution, volume, and age. New Zeal. J. Geol.

Geophys. 33, 89–109. https://doi.org/10.1080/00288306.1990.10427576
Gaetani, G.A., O'Leary, J.A., Shimizu, N., Bucholz, C.E., Newville, M., 2012. Rapid reequilibration of H2O and oxygen fugacity in olivine-hosted melt inclusions. Geology 40, 915–918. https://doi.org/10.1130/G32992.1
Gaetani, G.A., Watson, E.B., 2002. Modeling the major-element evolution of olivine-hosted melt inclusions. Chem. Geol. 183, 25–41. https://doi.org/10.1016/S0009-2541(01)00370-9
Gaetani, G.A., Watson, E.B., 2000. Open system behavior of olivine-hosted melt inclusions. Earth Planet. Sci. Lett. 183, 27–41. https://doi.org/10.1016/S0012-821X(00)00260-0
Gamble, J.A., Smith, I.E.M., Graham, I.J., Peter Kokelaar, B., Cole, J.W., Houghton, B.F., Wilson, C.J.N., 1990. The petrology, phase relations and tectonic setting of basalts from the taupo volcanic zone, New Zealand and the Kermadec Island arc - havre trough, SW Pacific. J. Volcanol. Geotherm. Res. 43, 253–270. https://doi.org/10.1016/0377-0273(90)90055-K
Gamble, J.A., Smith, I.E.M., McCulloch, M.T., Graham, I.J., Kokelaar, B.P., 1993. The geochemistry and petrogenesis of basalts from the Taupo Volcanic Zone and Kermadec Island Arc, S.W. Pacific. J. Volcanol. Geotherm. Res. 54, 265–290. https://doi.org/10.1016/0377-0273(93)90067-2
Gennaro, E., Paonita, A., Iacono-Marziano, G., Moussallam, Y., Pichavant, M., Peters, N., Martel, C., 2021. Sulphur Behaviour and Redox Conditions in Etnean Magmas during Magma Differentiation and Degassing. J. Petrol. 61. https://doi.org/10.1093/PETROLOGY/EGAA095
Graham, I.J., Cole, J.W., Briggs, R.M., Gamble, J.A., Smith, I.E.M., 1995. Petrology and petrogenesis of volcanic rocks from the Taupo Volcanic Zone: a review. J. Volcanol. Geotherm. Res. 68, 59–87. https://doi.org/10.1016/0377-0273(95)00008-I
Grange, L.I., 1937. The geology of the Rotorua-Taupo Subdivision, Rotorua and Kaimanawa Divisions. New Zeal. Geol. Surv. Bull. 37, 1–138.
Grove, T.L., Till, C.B., Krawczynski, M.J., 2012. The Role of H2O in Subduction Zone Magmatism. http://dx.doi.org/10.1146/annurev-earth-042711-105310 40, 413–439. https://doi.org/10.1146/ANNUREV-EARTH-042711-105310
Hamada, M., Fujii, T., 2007. H2O-rich island arc low-K tholeiite magma inferred from Ca-rich plagioclase-melt inclusion equilibria. Geochemical Journal2 41, 437–461.
Hamling, I.J., Kilgour, G., 2020. Goldilocks conditions required for earthquakes to trigger basaltic eruptions: Evidence from the 2015 Ambrym eruption. Sci. Adv. 6, eaaz5261. https://doi.org/10.1126/SCIADV.AAZ5261
Hartley, M.E., Maclennan, J., Edmonds, M., Thordarson, T., 2014. Reconstructing the deep CO2 degassing behaviour of large basaltic fissure eruptions. Earth Planet. Sci. Lett. 393, 120–131. https://doi.org/10.1016/j.epsl.2014.02.031
Hartley, M.E., Neave, D.A., Maclennan, J., Edmonds, M., Thordarson, T., 2015. Diffusive over-hydration of olivine-hosted melt inclusions. Earth Planet. Sci. Lett. 425, 168–178. https://doi.org/10.1016/J.EPSL.2015.06.008
Heise, W., Caldwell, T.G., Bertrand, E.A., Hill, G.J., Bennie, S.L., Palmer, N.G., 2016. Imaging the deep source of the Rotorua and Waimangu geothermal fields, Taupo Volcanic Zone, New Zealand. J. Volcanol. Geotherm. Res. 314, 39–48. https://doi.org/10.1016/j.jvolgeores.2015.10.017
Heise, W., Caldwell, T.G., Bibby, H.M., Bennie, S.L., 2010. Three-dimensional electrical resistivity image of magma beneath an active continental rift, Taupo Volcanic Zone, New Zealand. Geophys. Res. Lett. 37, n/a-n/a. https://doi.org/10.1029/2010GL043110
Hiess, J., Cole, J.W., Spinks, K.D., 2007. Influence of the crust and crustal structure on the location and composition of high-alumina basalts of the Taupo Volcanic Zone, New Zealand. New Zeal. J. Geol. Geophys. 50, 327–342. https://doi.org/10.1080/00288300709509840
Hopkins, J.L., Lowe, D.J., Horrocks, J.L., 2021. Tephrochronology in Aotearoa New Zealand. https://doi.org/10.1080/00288306.2021.1908368 64, 153–200. https://doi.org/10.1080/00288306.2021.1908368
Houghton, B.F., Hackett, W.R., 1984. Strombolian and phreatomagmatic deposits of Ohakune craters, Ruapehu, New Zealand: A complex interaction between external water and rising basaltic magma. J. Volcanol. Geotherm. Res. 21, 207–231. https://doi.org/10.1016/0377-0273(84)90023-4
Houghton, B.F., Wilson, C.J.N., 1989. A vesicularity index for pyroclastic deposits. Bull. Volcanol. 51, 451–462. https://doi.org/10.1007/BF01078811
Houghton, B.F., Wilson, C.J.N., McWilliams, M.O., Lanphere, M.A., Weaver, S.D., Briggs, R.M., Pringle, M.S., 1995. Chronology and dynamics of a large silicic magmatic system: central Taupo Volcanic Zone, New Zealand. Geology 23, 13–16. https://doi.org/10.1130/0091-7613(1995)023<0013:CADOAL>2.3.CO;2
Hughes, E.C., Buse, B., Kearns, S.L., Blundy, J.D., Kilgour, G., Mader, H.M., 2019a. Low analytical totals in EPMA of hydrous silicate glass due to sub-surface charging: Obtaining accurate volatiles by difference.

Chem. Geol. 505, 48–56. https://doi.org/10.1016/J.CHEMGEO.2018.11.015
Hughes, E.C., Mazot, A., Kilgour, G., Asher, C., Michelini, M., Britten, K., Chardot, L., Feisel, Y., Werner, C., 2019b. Understanding Degassing Pathways Along the 1886 Tarawera (New Zealand) Volcanic Fissure by Combining Soil and Lake CO2 Fluxes. Front. Earth Sci. 7, 264. https://doi.org/10.3389/feart.2019.00264
Iacovino, K., Till, C., 2018. DensityX: A program for calculating the densities of hydrous magmatic liquids from 427-1,627 °C and up to 30 kbar. Volcanica 2, 1–10. https://doi.org/10.30909/vol.02.01.0110
Jackson, M.D., Blundy, J., Sparks, R.S.J., 2018. Chemical differentiation, cold storage and remobilization of magma in the Earth's crust. Nature 564, 405–409. https://doi.org/10.1038/s41586-018-0746-2
Johnson, E.R., Kamenetsky, V.S., McPhie, J., Wallace, P.J., 2011. Degassing of the H2O-rich rhyolites of the Okataina Volcanic Center, Taupo Volcanic Zone, New Zealand. Geology 39, 311–314. https://doi.org/10.1130/G31543.1
Kay, S.M., Coira, B.L., Caffe, P.J., Chen, C.H., 2010. Regional chemical diversity, crustal and mantle sources and evolution of central Andean Puna plateau ignimbrites. J. Volcanol. Geotherm. Res. 198, 81–111. https://doi.org/10.1016/J.JVOLGEORES.2010.08.013
Keam, R.F., 1988. Tarawera: The volcanic eruption of 10 June 1886 A.D. Published by the author, Auckland.
Koepke, J., Feig, S.T., Snow, J., Freise, M., 2004. Petrogenesis of oceanic plagiogranites by partial melting of gabbros: an experimental study. Contrib. to Mineral. Petrol. 146, 414–432. https://doi.org/DOI 10.1007/s00410-003-0511-9
Kress, V.C., Carmichael, I.S.E., 1991. The compressibility of silicate liquids containing Fe2O3 and the effect of composition, temperature, oxygen fugacity and pressure on their redox states. Contrib. to Mineral. Petrol. 108, 82–92. https://doi.org/10.1007/BF00307328
Laumonier, M., Scaillet, B., Pichavant, M., Champallier, R., Andujar, J., Arbaret, L., 2014. On the conditions of magma mixing and its bearing on andesite production in the crust. Nat. Commun. 2014 51 5, 1–12. https://doi.org/10.1038/ncomms6607
Law, S., Bromiley, G.D., Kilgour, G.N., Fitton, J.G., 2021. Tracing mantle source variation through xenocrystic olivine in the Taupo Volcanic Zone, New Zealand: A role for lithospheric mantle in the shift from andesitic to rhyolitic compositions. Lithos 394–395, 106185. https://doi.org/10.1016/J.LITHOS.2021.106185
Law, S., Kilgour, G., Bromiley, G.D., Boyce, A.J., n.d. Along arc variation in monogenetic mafic magmas from the Taupo Volcanic Zone, New Zealand: Insights from the crystal cargo and oxygen isotopes. J. Petrol.
Leonard, G.S., Cole, J.W., Nairn, I.A., Self, S., 2002. Basalt triggering of the c. AD 1305 Kaharoa rhyolite eruption, Tarawera Volcanic Complex, New Zealand. J. Volcanol. Geotherm. Res. 115, 461–486. https://doi.org/10.1016/S0377-0273(01)00326-2
Lloyd, A.S., Plank, T., Ruprecht, P., Hauri, E.H., Rose, W., 2013. Volatile loss from melt inclusions in pyroclasts of differing sizes. Contrib. to Mineral. Petrol. 165, 129–153. https://doi.org/10.1007/s00410-012-0800-2
Lowenstern, J.B., 2003. Melt inclusions come of age: Volatiles, volcanoes, and Sorby's legacy. Dev. Volcanol. 5, 1–21. https://doi.org/10.1016/S1871-644X(03)80021-9
Lowenstern, J.B., 1995. Applications of silicate-melt inclusions to the study of magmatic volatiles, in: Thompson, J.F.. (Ed.), Magmas, Fluids and Ore Deposits. Mineralogical Assoication of Canada Short Course Volume No.23. pp. 71–99.
Maclennan, J., 2017. Bubble formation and decrepitation control the CO2 content of olivine-hosted melt inclusions. Geochemistry, Geophys. Geosystems 18, 597–616. https://doi.org/10.1002/2016GC006633
Mangan, M.T., Sisson, T.W., Hankins, W. Ben, Shimizu, N., Vennemann, T., 2021. Constraints on deep, CO2-rich degassing at arc volcanoes from solubility experiments on hydrous basaltic andesite of Pavlof Volcano, Alaska Peninsula, at 300 to 1200 MPa. Am. Mineral. 106, 762–773. https://doi.org/10.2138/am-2021-7531
Mazot, A., Schwandner, F.M., Christenson, B., de Ronde, C.E.J., Inguaggiato, S., Scott, B.J., Graham, D., Britten, K., Keeman, J., Tan, K., 2014. CO2 discharge from the bottom of volcanic Lake Rotomahana, New Zealand. Geochemistry, Geophys. Geosystems 15, 577–588. https://doi.org/10.1002/2013GC004945
Moore, L.R., Gazel, E., Tuohy, R., Lloyd, A.S., Esposito, R., Steele-MacInnis, M., Hauri, E.H., Wallace, P.J., Plank, T., Bodnar, R.J., 2015. Bubbles matter: An assessment of the contribution of vapor bubbles to melt inclusion volatile budgets. Am. Mineral. 100, 806–823. https://doi.org/10.2138/am-2015-5036
Moretti, R., Métrich, N., Arienzo, I., Di Renzo, V., Aiuppa, A., Allard, P., 2018. Degassing vs. eruptive styles at Mt. Etna volcano (Sicily, Italy). Part I: Volatile stocking, gas fluxing, and the shift from low-energy to highly explosive basaltic eruptions. Chem. Geol. 482, 1–17. https://doi.org/10.1016/J.CHEMGEO.2017.09.017
Mortimer, N., Campbell, H.J., Tulloch, A.J., King, P.R., Stagpoole, V.M., Wood, R.A., Rattenbury, M.S., Sutherland, R., Adams, C.J., Collot, J., Seton, M., 2017. Zealandia: Earth's hidden Continent. GSA Today 27, 27–35. https://doi.org/10.1130/GSATG321A.1

Müntener, O., Ulmer, P., 2018. Arc crust formation and differentiation constrained by experimental petrology. Am. J. Sci. 318, 64–89. https://doi.org/10.2475/01.2018.04
Nairn, I.A., 2002. Geology of the Okataina Volcanic Centre, scale 1:50 000. Institute of Geological and Nuclear Sciences Limited.
Nairn, I.A., 1992. The Te Rere and Okareka eruptive episodes — Okataina Volcanic Centre, Taupo Volcanic Zone, New Zealand. New Zeal. J. Geol. Geophys. 35, 93–108. https://doi.org/10.1080/00288306.1992.9514503
Nairn, I.A., 1981. Some Studies of the Geology, Volcanic History, and Geothermal Resources of the Okataina Volcanic Centre, Taupo Volcanic Zone, New Zealand. Victoria University of Wellington, Wellington.
Nairn, I.A., 1979. Rotomahana—Waimangu eruption, 1886: base surge and basalt magma. New Zeal. J. Geol. Geophys. 22, 363–378. https://doi.org/10.1080/00288306.1979.10424105
Nairn, I.A., Cole, J.W., 1981. Basalt dikes in the 1886 Tarawera Rift. New Zeal. J. Geol. Geophys. 24, 585–592. https://doi.org/10.1080/00288306.1981.10421534
Nairn, I.A., Self, S., Cole, J.W., Leonard, G.S., Scutter, C., 2001. Distribution, stratigraphy, and history of proximal deposits from the c. AD 1305 Kaharoa eruptive episode at Tarawera Volcano, New Zealand. New Zeal. J. Geol. Geophys. 44, 467–484. https://doi.org/10.1080/00288306.2001.9514950
Nairn, I.A., Shane, P.A., Cole, J.W., Leonard, G.., Self, S., Pearson, N., 2004. Rhyolite magma processes of the ~AD 1315 Kaharoa eruption episode, Tarawera volcano, New Zealand. J. Volcanol. Geotherm. Res. 131, 265–294. https://doi.org/10.1016/S0377-0273(03)00381-0
Nandedkar, R.H., Ulmer, P., Müntener, O., 2014. Fractional crystallization of primitive, hydrous arc magmas: An experimental study at 0.7 GPa. Contrib. to Mineral. Petrol. 167, 1–27. https://doi.org/10.1007/s00410-014-1015-5
Neave, D.A., Putirka, K.D., 2017. A new clinopyroxene-liquid barometer, and implications for magma storage pressures under Icelandic rift zones. Am. Mineral. 102, 777–794. https://doi.org/10.2138/am-2017-5968
Nielsen, R.L., Michael, P.J., Sours-Page, R., 1998. Chemical and physical indicators of compromised melt inclusions. Geochim. Cosmochim. Acta 62, 831–839. https://doi.org/10.1016/S0016-7037(98)00024-6
O'Neill, H., 2020. The thermodynamic controls on sulfide saturation in silicate melts with application to Ocean Floor Basalts. https://doi.org/10.1002/ESSOAR.10503096.1
Panjasawatwong, Y., Danyushevsky, L. V., Crawford, A.J., Harris, K.L., 1995. An experimental study of the effects of melt composition on plagioclase-melt equilibria at 5 and 10 kbar: implications for the origin of magmatic high-An plagioclase. Contrib. to Mineral. Petrol. 118, 420–432. https://doi.org/10.1007/s004100050024
Pérez, W., Freundt, A., Kutterolf, S., 2020. The basaltic plinian eruption of the ~6 ka San Antonio Tephra and formation of the Masaya caldera, Nicaragua. J. Volcanol. Geotherm. Res. 401, 106975. https://doi.org/10.1016/j.jvolgeores.2020.106975
Pittari, A., Muir, S.L., Hendy, C.H., 2016. Lake-floor sediment texture and composition of a hydrothermally-active, volcanic lake, Lake Rotomahana. J. Volcanol. Geotherm. Res. 314, 169–181. https://doi.org/10.1016/j.jvolgeores.2016.02.025
Price, R.C., Gamble, J.A., Smith, I.E.M., Stewart, R.B., Eggins, S., Wright, I.C., 2005. An integrated model for the temporal evolution of andesites and rhyolites and crustal development in New Zealand's North Island. J. Volcanol. Geotherm. Res. 140, 1–24. https://doi.org/10.1016/j.jvolgeores.2004.07.013
Pullar, W.A., Nairn, I.A., 1972. Matahi Basaltic Tephra member, Rotoiti Breccia Formation. New Zeal. J. Geol. Geophys. 15, 446–450. https://doi.org/10.1080/00288306.1972.10422342
Putirka, K.D., 2008. Thermometers and Barometers for Volcanic Systems. Rev. Mineral. Geochemistry 69, 61–120. https://doi.org/10.2138/rmg.2008.69.3
Rasmussen, D.J., Plank, T.A., Wallace, P.J., Newcombe, M.E., Lowenstern, J.B., 2020. Vapor-bubble growth in olivine-hosted melt inclusions. Am. Mineral. 105, 1898–1919. https://doi.org/10.2138/am-2020-7377
Roedder, E., 1979. Origin and significance of magmatic inclusions. Bull. Mineral. 102, 487–510.
Rooney, T.O., Deering, C.D., 2014. Conditions of melt generation beneath the Taupo Volcanic Zone: The influence of heterogeneous mantle inputs on large-volume silicic systems. Geology 42, 3–6. https://doi.org/10.1130/G34868.1
Rooyakkers, S.M., Wilson, C.J.N., Schipper, C.I., Barker, S.J., Allan, A.S.R., 2018. Textural and micro-analytical insights into mafic–felsic interactions during the Oruanui eruption, Taupo. Contrib. to Mineral. Petrol. 173, 35. https://doi.org/10.1007/s00410-018-1461-6
Rose-Koga, E.F., Bouvier, A.S., Gaetani, G.A., Wallace, P.J., Allison, C.M., Andrys, J.A., Angeles de la Torre, C.A., Barth, A., Bodnar, R.J., Bracco Gartner, A.J.J., Butters, D., Castillejo, A., Chilson-Parks, B., Choudhary, B.R., Cluzel, N., Cole, M., Cottrell, E., Daly, A., Danyushevsky, L. V., DeVitre, C.L., Drignon, M.J., France, L., Gaborieau, M., Garcia, M.O., Gatti, E., Genske, F.S., Hartley, M.E., Hughes, E.C., Iveson, A.A., Johnson, E.R., Jones, M., Kagoshima, T., Katzir, Y., Kawaguchi, M., Kawamoto, T., Kelley, K.A., Koornneef, J.M., Kurz, M.D., Laubier, M., Layne, G.D., Lerner, A., Lin, K.Y., Liu, P.P.,

Lorenzo-Merino, A., Luciani, N., Magalhães, N., Marschall, H.R., Michael, P.J., Monteleone, B.D., Moore, L.R., Moussallam, Y., Muth, M., Myers, M.L., Narváez, D.F., Navon, O., Newcombe, M.E., Nichols, A.R.L., Nielsen, R.L., Pamukcu, A., Plank, T., Rasmussen, D.J., Roberge, J., Schiavi, F., Schwartz, D., Shimizu, K., Shimizu, N., Thomas, J.B., Thompson, G.T., Tucker, J.M., Ustunisik, G., Waelkens, C., Zhang, Y., Zhou, T., 2021. Silicate melt inclusions in the new millennium: A review of recommended practices for preparation, analysis, and data presentation. Chem. Geol. 570, 120145. https://doi.org/10.1016/j.chemgeo.2021.120145

Rowe, M.C., Carey, R.J., White, J.D.L., Kilgour, G., Hughes, E., Ellis, B., Rosseel, J.-B., Segovia, A., 2021. Tarawera 1886: an integrated review of volcanological and geochemical characteristics of a complex basaltic eruption. New Zeal. J. Geol. Geophys. 64, 296–319. https://doi.org/10.1080/00288306.2021.1914118

Sable, J.E., Houghton, B.F., Wilson, C.J.N., Carey, R.J., 2009. Eruption Mechanisms during the climax of the Tarawera 1886 basaltic Plinian eruption inferred from microtextural characteristics of the deposits, in: Thordarson, T., Self, S., Larsen, G., Rowland, S.K., Hoskuldsson, A. (Eds.), Studies in Volcanology: The Legacy of John Walker. The Geological Society of London, London, pp. 129–154.

Saper, L.M., Stolper, E.M., 2020. Controlled Cooling-Rate Experiments on Olivine-Hosted Melt Inclusions: Chemical Diffusion and Quantification of Eruptive Cooling Rates on Hawaii and Mars. Geochemistry, Geophys. Geosystems 21. https://doi.org/10.1029/2019GC008772

Sas, M., Shane, P., Kuritani, T., Zellmer, G.F., Kent, A.J.R., Nakagawa, M., 2021. Mush, melts and metasediments: A history of rhyolites from the Okataina Volcanic Centre, New Zealand, as captured in plagioclase. J. Petrol. https://doi.org/10.1093/petrology/egab038

Schiano, P., 2003. Primitive mantle magmas recorded as silicate melt inclusions in igneous minerals. Earth-Science Rev. 63, 121–144. https://doi.org/10.1016/S0012-8252(03)00034-5

Schmitz, M.D., Smith, I.E.M., 2004. The Petrology of the Rotoiti Eruption Sequence, Taupo Volcanic Zone: an Example of Fractionation and Mixing in a Rhyolitic System. J. Petrol. 45, 2045–2066. https://doi.org/10.1093/petrology/egh047

Seebeck, H., Nicol, A., Stern, T.A., Bibby, H.M., Stagpoole, V., 2010. Fault controls on the geometry and location of the Okataina Caldera, Taupo Volcanic Zone, New Zealand. J. Volcanol. Geotherm. Res. 190, 136–151. https://doi.org/10.1016/J.JVOLGEORES.2009.04.011

Seropian, G., Kennedy, B.M., Walter, T.R., Ichihara, M., Jolly, A.D., 2021. A review framework of how earthquakes trigger volcanic eruptions. Nat. Commun. 12, 1–13. https://doi.org/10.1038/s41467-021-21166-8

Shane, P.A., Martin, S.B., Smith, V.C., Beggs, K.F., Darragh, M.B., Cole, J.W., Nairn, I.A., 2007. Multiple rhyolite magmas and basalt injection in the 17.7 ka Rerewhakaaitu eruption episode from Tarawera volcanic complex, New Zealand. J. Volcanol. Geotherm. Res. 164, 1–26. https://doi.org/10.1016/j.jvolgeores.2007.04.003

Shane, P.A., Nairn, I.A., Smith, V.C., 2005. Magma mingling in the ~50 ka Rotoiti eruption from Okataina Volcanic Centre: implications for geochemical diversity and chronology of large volume rhyolites. J. Volcanol. Geotherm. Res. 139, 295–313. https://doi.org/10.1016/j.jvolgeores.2004.08.012

Shane, P.A., Nairn, I.A., Smith, V.C., Darragh, M.B., Beggs, K.F., Cole, J.W., 2008a. Silicic recharge of multiple rhyolite magmas by basaltic intrusion during the 22.6 ka Okareka Eruption Episode, New Zealand. Lithos 103, 527–549. https://doi.org/10.1016/j.lithos.2007.11.002

Shane, P.A., Smith, V.C., Nairn, I.A., 2008b. Millennial timescale resolution of rhyolite magma recharge at Tarawera volcano: insights from quartz chemistry and melt inclusions. Contrib. to Mineral. Petrol. 156, 397–411. https://doi.org/10.1007/s00410-008-0292-2

Smith, V.C., Shane, P., Nairn, I.A., 2004. Reactivation of a rhyolitic magma body by new rhyolitic intrusion before the 15.8 ka Rotorua eruptive episode: implications for magma storage in the Okataina Volcanic Centre, New Zealand. J. Geol. Soc. London. 161, 757–772. https://doi.org/10.1144/0016-764903-092

Smith, V.C., Shane, P.A., Nairn, I.A., 2005. Trends in rhyolite geochemistry, mineralogy, and magma storage during the last 50 kyr at Okataina and Taupo volcanic centres, Taupo Volcanic Zone, New Zealand. J. Volcanol. Geotherm. Res. 148, 372–406. https://doi.org/10.1016/j.jvolgeores.2005.05.005

Sobolev, A. V., Shimizu, N., 1993. Ultra-depleted primary melt included in an olivine from the Mid-Atlantic Ridge. Nature 363, 151–154. https://doi.org/10.1038/363151a0

Sparks, S.R.J., Sigurdsson, H., Wilson, L., 1977. Magma mixing: a mechanism for triggering acid explosive eruptions. Nat. 1977 2675609 267, 315–318. https://doi.org/10.1038/267315a0

Storm, S., Shane, P., Schmitt, A.K., Lindsay, J.M., 2011. Contrasting punctuated zircon growth in two syn-erupted rhyolite magmas from Tarawera volcano: Insights to crystal diversity in magmatic systems. Earth Planet. Sci. Lett. 301, 511–520. https://doi.org/10.1016/J.EPSL.2010.11.034

Takagi, D., Sato, H., Nakagawa, M., 2005. Experimental study of a low-alkali tholeiite at 1-5 kbar: Optimal condition for the crystallization of high-An plagioclase in hydrous arc tholeiite. Contrib. to Mineral.

Petrol. 149, 527–540. https://doi.org/10.1007/s00410-005-0666-7
Tattitch, B., Chelle-Michou, C., Blundy, J., Loucks, R.R., 2021. Chemical feedbacks during magma degassing control chlorine partitioning and metal extraction in volcanic arcs. Nat. Commun. 2021 121 12, 1–11. https://doi.org/10.1038/s41467-021-21887-w
Thomas, A.P.W., 1888. Report on the Eruption of Tarawera and Rotomahana, NZ, Government Printer, Wellington, New Zealand.
Thomas, R.W., Wood, B.J., 2021. The chemical behaviour of chlorine in silicate melts. Geochim. Cosmochim. Acta 294, 28–42. https://doi.org/10.1016/J.GCA.2020.11.018
Walker, G.P.L., Self, S., Wilson, L., 1984. Tarawera 1886, New Zealand — A basaltic plinian fissure eruption. J. Volcanol. Geotherm. Res. 21, 61–78. https://doi.org/10.1016/0377-0273(84)90016-7
Wallace, P.J., 2005. Volatiles in subduction zone magmas: concentrations and fluxes based on melt inclusion and volcanic gas data. J. Volcanol. Geotherm. Res. 140, 217–240. https://doi.org/10.1016/j.jvolgeores.2004.07.023
Wallace, P.J., Kamenetsky, V.S., Cervantes, P., 2015. Melt inclusion CO2 contents, pressures of olivine crystallization, and the problem of shrinkage bubbles. Am. Mineral. 100, 787–794. https://doi.org/10.2138/am-2015-5029
Waters, L.E., Lange, R.A., 2015. An updated calibration of the plagioclase-liquid hygrometer-thermometer applicable to basalts through rhyolites. Am. Mineral. 100, 2172–2184. https://doi.org/10.2138/AM-2015-5232
Williams, S.N., 1983. Plinian airfall deposits of basaltic composition. Geology 11, 211–214. https://doi.org/10.1130/0091-7613(1983)11
Wilson, C.J.N., Blake, S., Charlier, B.L.A., Sutton, A.N., 2006. The 26·5 ka Oruanui Eruption, Taupo Volcano, New Zealand: Development, Characteristics and Evacuation of a Large Rhyolitic Magma Body. J. Petrol. 47, 35–69. https://doi.org/10.1093/petrology/egi066
Wilson, C.J.N., Houghton, B.F., McWilliams, M.O., Lanphere, M.A., Weaver, S.D., Briggs, R.M., 1995. Volcanic and structural evolution of Taupo Volcanic Zone, New Zealand: a review. J. Volcanol. Geotherm. Res. 68, 1–28. https://doi.org/10.1016/0377-0273(95)00006-G
Wysoczanski, R.J., Wright, I.C., Gamble, J.A., Hauri, E.H., Luhr, J.F., Eggins, S.M., Handler, M.R., 2006. Volatile contents of Kermadec Arc–Havre Trough pillow glasses: Fingerprinting slab-derived aqueous fluids in the mantle sources of arc and back-arc lavas. J. Volcanol. Geotherm. Res. 152, 51–73. https://doi.org/10.1016/J.JVOLGEORES.2005.04.021
Zellmer, G.F., Kimura, J.-I., Stirling, C.H., Lube, G., Shane, P.A., Iizuka, Y., 2020. Genesis of recent mafic magmatism in the Taupo Volcanic Zone, New Zealand: insights into the birth and death of very large volume rhyolitic systems? J. Petrol. 61, egaa027. https://doi.org/10.1093/petrology/egaa027